Design Exploration and Optimization for Long-Span Curved CLT Shell Components Enabled Through Low-Grade Fiber Source

by

Rilynn Zarate

A thesis accepted and approved in partial fulfillment of the

requirements for the degree of

Master of Science

in Architecture

Thesis Committee:

Dylan Wood, Chair

Judith Sheine, Member

Lech Muszynski, Member

University of Oregon

Summer 2026

© 2026 Rilynn Zarate
This work is openly licensed via CC BY 4.0



THESIS ABSTRACT

Rilynn Zarate

Master of Science in Architecture

Title: Design Exploration and Optimization for Long-Span Curved CLT Shell Components Enabled Through Low-Grade Fiber Source

Demand for mass timber products is projected to increase in the future and to meet this need ecologically, a shift in both material efficiency and fiber sources used in these products is necessary. One under-utilized fiber source is wood from small-diameter trees (SDT), harvested during forest restoration thinning operations which the US Forest Service is seeking higher-value product streams to offset harvesting costs, including use of lamstock, in cross laminated timber (CLT). Boards milled from SDT can also produce smaller dimensioned lumber, or "thins" and "narrows," these currently have few structural applications. Additionally, thinner and narrower boards tend to bend and twist more than standard dimensional lumber, which is typically viewed as a problem, however this makes them ideal for forming into doubly curved, highly efficient, thin shell CLT ceiling panels. Answering the research question, is it possible to leverage curved geometry to increase the material efficiency of CLT; this study examines a digital geometry optimization approach for curved thin shell CLT panels that seek structural and material efficiency improvements when compared to typical rectilinear one-way post and beam CLT systems. This optimized geometry is evaluated based on the approximate material parameters of "thins" and "narrows" from SDT with simulated and prototype testing through a hypothetical design scenario of a long-span case study. This design process resulted in a digital workflow that incorporates multi-objective geometry optimizations, initial design phase structural analysis, project specific machine learning statistical analysis, fiber source specific manufacturability checks, and a 1:1 prototype of a segment of an optimized long-span curved CLT shell.

ACKNOWLEDGMENTS

This research was made possible by the many dedicated faculty and students at the University of Oregon's School of Architecture and Environment in the College of Design and Oregon State University's Department of Wood Science and Engineering in the College of Forestry.

Thank you to my Committee Dylan Wood, Judith Sheine, and Lech Muszynski for helping shape this project, for giving me the confidence to execute it, and all the constructive feedback each of you has given along the way. I would like to thank my Committee Chair, Dylan Wood for bringing me into the world of mass timber research and always challenging me to dig deeper. Thank you to Judith Sheine for helping to keep this research grounded and for all the valuable advice you have given throughout this project.

I would also like to thank the incredibly helpful woodshop staff who made the physical tests possible. A special thanks to Tom Cotes who helped teach me to use the tools safely, for operating the CNC machine, and for all the woodworking tips you have shared.

Thank you to my cohort, Helene Brehl and Ethan Frolov for the camaraderie and support as we went through this process together. A special thanks to Ethan Frolov for always offering to help throughout the fabrication process.

Thank you to Marco Zarate for always providing a helping hand in the woodshop, with heavy lifting, and with panel fabrication.

DEDICATION

This research is dedicated to my children, Olivia and Aria, my biggest cheerleaders, and my reason why.

TABLE OF CONTENTS

Chapter	Page
I. INTROCDUCTION	12
1.1 Motivation	12
1.2 Opportunity	13
1.3 Organization of Thesis	15
1.4 Background	16
1.5 Research Question	20
II. GOALS AND OBJECTIVES	22
2.1 Goals and Objectives	22
III. MATERIALS AND METHODS	23
3.1 General Methodology	23
3.2 Geometry Generation and Parametric Model Selection	25
3.3 Optimization Solution-Space Analysis	31
3.4 Material-Specific Fabrication Feasibility Analysis	35
3.5 Fabrication and Prototyping	38

Chapter Page

IV. RESULTS 41

4.1 Geometry Generation Model and Data Selection 41

4.2 Long-Span Application Case Study 41

4.2 Prototyping and Fabrication 54

4.3 Design Implications 57

V. CONCLUSION 59

5.1 Summary 59

5.2 Limitations and Future Work 60

5.3 Impact 60

APPENDIX: PHYSICAL PROTOYPE FABRICATION PROCESS IMAGES 63

VII. REFERENCES CITED 67

LIST OF FIGURES

Figure Page

1. Value-added product and material efficiency opportunities 13

2. Shell curvature types 13

3. Physical wood bending and twisting 14

4. Diagonal layup and wood bending 15

5. Forest density, log diameter, and SDT 16

6. Forest restoration thinning 17

7. Digital workflow general methods 23

8. Karamba configuration 24

9. Geometry Model Screening Phases 26

10. Parametric geometry creation process 27

11. Geometry generation models 28

12. Visual comparison of layer series 30

13. 3R5P Geometry generation model 31

14. Diagram of Pareto analysis scatter plot 33

15. Diagram of near-Pareto analysis 34

16. Diagram of k-means clustering 34

17. Cluster Z-height variation analysis diagram 35

18. Lamella bending feasibility check process 36

19. Curvature fabrication feasibility analysis 37

20. 1:4 scale prototype layup 39

21. 1:1 scale prototype X-configuration layup 40

22. 1:1 panel geometry selection 40

23. Final geometry model selection 41

24. Data selection diagram 42

25. Nine-layer series Pareto analysis 46

26. Nine-layer series family gallery 47

27. Nine-layer series cluster analysis graph 47

28. Ten-layer series Pareto analysis 48

29. Ten-layer series cluster analysis graph 49

30. Ten-layer series family gallery 49

31. Dominant family comparison 50

32. Geometric outliers 51

33. Iteration 163 and 285 on Pareto-front 51

34. Curvature analysis comparison 52

35. Edge condition comparison 53

36. 1:4 physical prototype X-configuration panel 55

37. 1:1 lamella bending feasibility check 56

38. 1:1 Physical prototype 56

39. Airport section 57

40. Volume comparison setup 58

41. Airport render exterior 61

42. Airport render interior 62

43. Successful 1:1 panel fabrication 62

44. Diagonal layup layer for 1:4 scale prototype 63

45. Identifying fabrication process problems..... 63

46. Small fabrication process test 64

47. X-configuration layer..... 64

48. Testing new fabrication process..... 65

49. Process to secure 1:1 panel to the mold..... 66

50. 1:1 digital geometry vs. physical prototype comparison 66

LIST OF TABLES

Table Page

1. MOO result comparison..... 43

CHAPTER I
INTRODUCTION

1.1 Motivation

With increasing demand for engineered wood products in building construction [11, 17, 47], one study projects that the current land use area for timber plantations would need to double or triple by the end of the century to meet this need [40]. Wood harvested during thinning can be used to mitigate deficits while new plantations are established to continue benefiting from the carbon storage of wood construction [40, 42]. Sustainable forestry will produce greater quantities of small, low-value timber stock, which is expensive to harvest and lacks high-value product output streams [68]. Increasingly, small-diameter trees (SDT), are being harvested in thinning operations aimed at improving forest health and fire resistance. These logs are typically 8" or less in diameter and are turned into low-value products like chips, paper, veneer, or fuel pellets [15, 42]. If milled into boards, SDT can produce "thins" and "narrows," or boards that are smaller than the typical 2x4's or 2x6's which tend to be used for higher-value structural purposes [4, 44, 48, 72].

Government agencies like the US Forest Service are looking for value-added products to offset the expense of their forest restoration thinning program [68]. According to a 2005 study conducted on an overstocked forest harvest of SDT, 49% of boards milled from these trees met grading and structural performance standards when tested for use in laminated wood products [21]. Further, Muszynski discusses the success of plywood and other laminated wood products like cross laminated timber (CLT) that improve the performance, both structurally and monetarily, of wood from SDT [42]. However, the post and beam structural system dominating mass timber construction [30] is materially inefficient with some analysis suggesting that beams with rectangular cross sections utilize only 33% of their capacity [1]. Additionally, due to current manufacturing and sourcing practices, higher grade lamella are used in CLT and other mass timber products despite being able to be made with lower grade fiber stock [7, 15, 26].

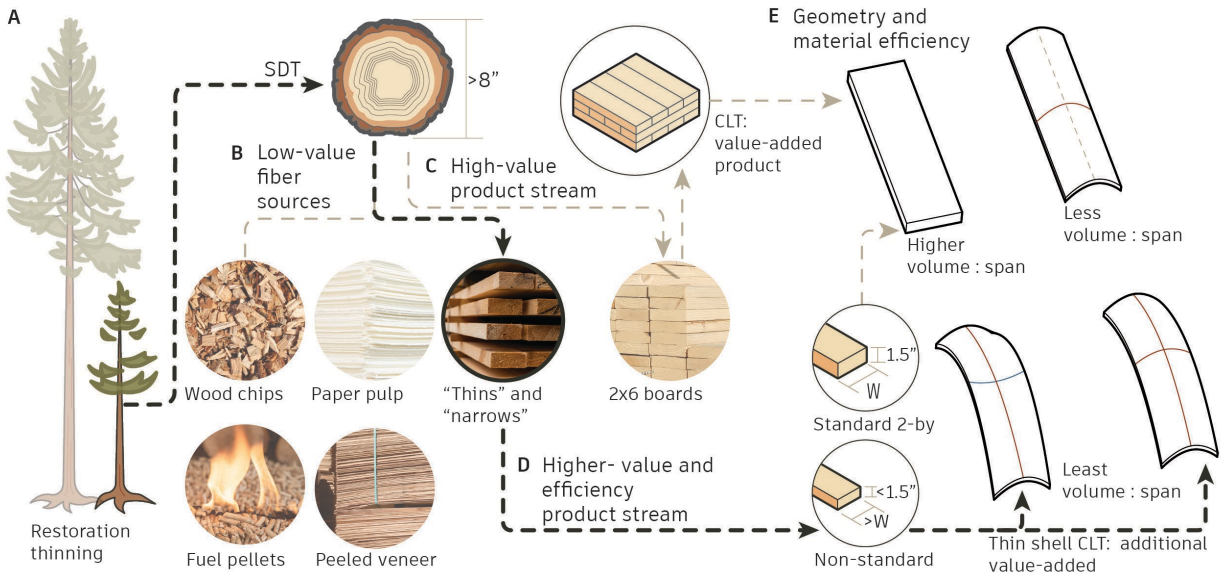


Figure 1. Value-added product and material efficiency opportunities: A.) forest restoration thinning producing SDT logs B.) low-value fiber sources from SDT C.) a current high-value product stream for standard dimensional lumber milled from SDT D.) proposed higher-value and material efficient product stream for "thins" and "narrows" or non-standard dimensional lumber from SDT E.) curved geometry can achieve spans for less material then compared to rectilinear panels CLT typically makes

1.2 Opportunity

Structural and material usage benefits of curvature in architecture are well known through examples like arches, vaults, and domes. Optimization of synclastic or anticlastic (Figure 2) thin shell structures, especially with the help of digital finite element analysis, further improves on these efficiencies [49]. In addition to structural improvements, there are embodied carbon reduction and material efficiency benefits from curving structural wood panels [24]. Despite this improvement, double curvature in mass timber is typically only used for parallel grain laminations like glulam, or in cross lamination for non-structural or furniture applications with thin veneer layers like plywood [43, 64, 73]. The thick and wide lamella used in CLT can make it difficult to bend and twist to mold to more complicated double curved geometries.



Figure 2. Shell curvature types: A.) monoclastic B.) synclastic C.) anticlastic

The relationship between decreased radius of bent wood as its thickness decreases is well studied [19, 46, 59]. Leveraging lamella that are both thin and narrow (Figure 3), glulam can achieve both a small radius and the torsion in complex double curved beams [60]. However, American standards for curved glulam advise against using these lamellae thinner than 1" due to the increased waste produced in sawdust during milling [70]. Lamella width in CLT is governed by the thickness to width ratios (1:1.75 in the longitudinal direction) making torsion in panels dependent on how thin the lamella can be [74]. SDT, if milled into boards, already produces non-standard board dimensions or 'thins' and 'narrows' which are smaller than the standard 2x6's typically used in CLT [44, 68, 72]. This makes these boards that are already thinner and narrower than standard dimensional lumber well suited for both bending and twisting into a wider range of potential curvature configurations in CLT panels. This is done without needing to re-mill standard dimensional boards which produce additional waste in sawdust.

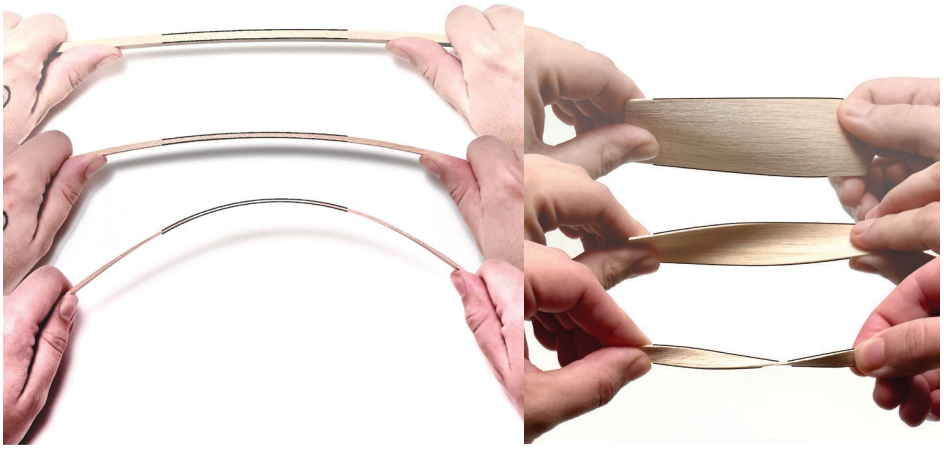


Figure 3. Physical wood bending and twisting: representations of how thinness and narrowness impacts bending and twisting of wood

Considering thin shells as being an efficient structural system for point supported long-span applications [49] a curved CLT shell panel's dimensions would be significantly shorter in the transverse direction than the longitudinal direction due to transportation limitations [12]. This creates a problem where the curvature in the transverse direction could exceed minimum possible radius for bent wood leading to failure or breakage of lamella during the molding process (Figure 4). Typical CLT uses a layup of an odd number of lamella layers with each layer being perpendicular to the layer under it. In recent years, more research has been done exploring

diagonal layup (DL) CLT that uses longitudinal layers separated by layers rotated only 30°-40° instead of the typical 90°. Not only has this layup method been found to improve panel torsional stiffness, but it has also been found to need fewer layers and, therefore, less material to achieve this improved mechanical performance [2, 33]. Diagonal layup for CLT creates an opportunity to avoid placing lamella directly over tight transverse radius in a curved panel's geometry. Instead, rotating lamella diagonally increases the bending radius the board is being bent to which also reduces the risk of breaking boards.

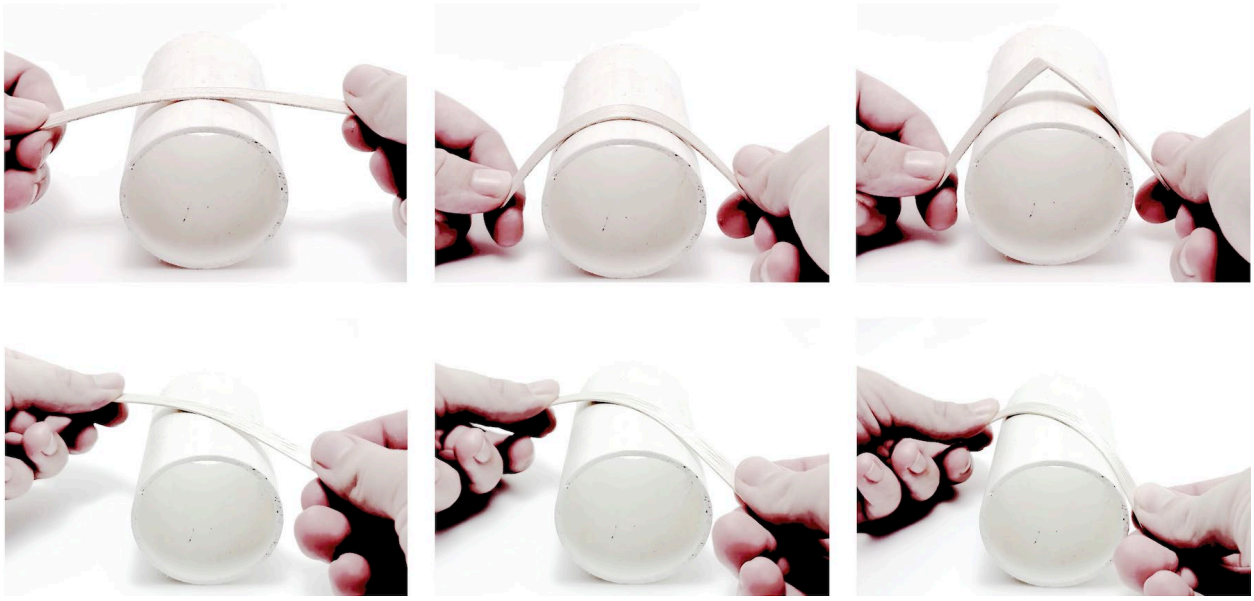


Figure 4. Diagonal layup and wood bending: representation comparing breaking in the transverse direction versus a diagonal layup approach.

1.3 Organization of Thesis

This thesis is organized into five chapters. Chapter 1 introduces motivation and opportunity, opportunity, establishes the background, and presents the research question guiding the study. Chapter 2 defines the goals and objectives of this research. Chapter 3 describes the materials and methods used to develop and evaluate the digital workflow, including geometry generation, multi-objective optimization, solution-space analysis, fabrication feasibility checks, and physical prototyping. Chapter 4 presents the results of the geometry generation model selection, long-span application case study, fabrication and prototyping, and resulting design implications. Finally, Chapter 5 summarizes the findings of the study and discusses its limitations, potential impact, and opportunities for future work.

1.4 Background

1.4.2 Low-Value Fiber and Product Streams

The U.S adopted a policy of fire suppression beginning in the early 1900s which directly contradicted the pre-existing natural fire frequency evident in studies conducted on fire scarring on old growth timber [57]. Between 1911 and 2011 western forests have seen forest stand density increase 6-7 times simultaneously with an average log diameter decrease of 50% (Figure 5) and a general downward trend in health and resiliency [45]. A 2015 analysis identifying forest restoration needs for Oregon and Washington coniferous forests found that 40% of forest acreage needed new restoration measures with roughly 80% of that acreage requiring thinning for fire mitigation [22]. By removing SDT that grow in these overstocked forests (Figure 6), fire hazards can be reduced while also reducing competition amongst trees promoting growth of larger healthier timber stock [15]

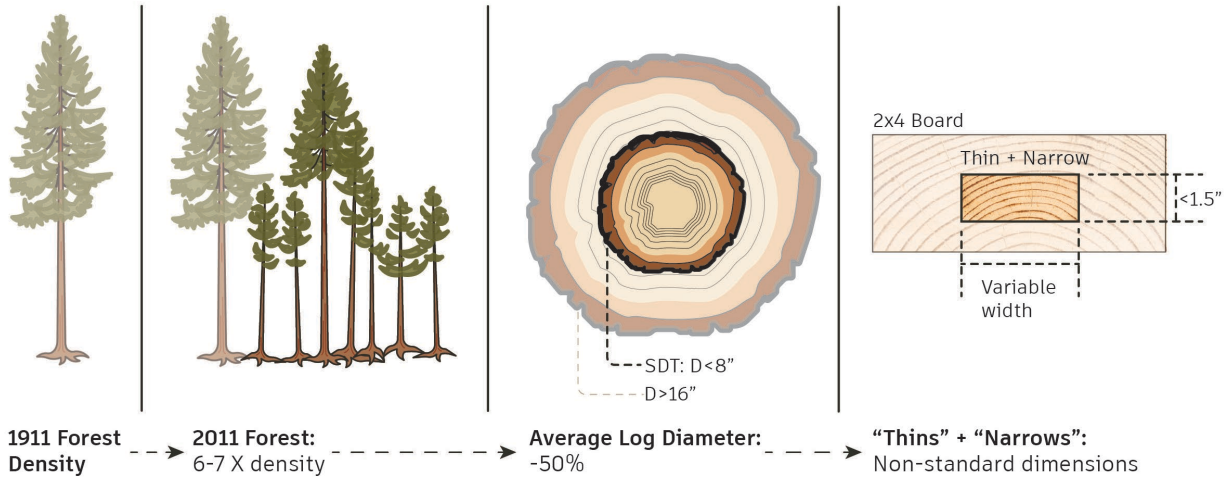


Figure 5. Forest density, log diameter, and SDT: depiction of the impact of fire restriction of forest density which has led to increased SDT which produce "thins" and "Narrows"

However beneficial this practice of selectively harvesting SDT may be, the extraction process can be expensive, mills are not always equipped for small logs, and there are few profitable product streams for its use [68]. Current practice for processing SDT is to turn it into chips, pulp for paper, mill it into boards if the log is large enough, or peel it for veneers. When SDT is milled into boards, it often produces "thins" and "narrows" or <1.5" thick boards with variations in widths [4, 16]. Most of these products are considered low-value and do have value-added uses in examples like flooring, furniture, composites, or other engineered wood products [35]. Several studies have been conducted that highlight both the profitability and restoration

benefits of utilizing wood from SDT in engineered wood products like mass plywood panels (MPP), glulam, or CLT [21, 31, 42]. One study looks at the structural performance of CLT panels using thin lamella harvested from small-diameter ponderosa pine and optimizes a custom layup for the minimum lamella thickness, within standards, for a specific design scenario [27]. These studies do not consider the inherent material inefficiencies of large rectilinear structural systems like CLT.



Figure 6. Forest restoration thinning: selective harvesting of dense strand to remove SDT improving forest health and fire resiliency

1.4.3 CLT and Material Efficiencies

The concept behind CLT, using adhesives to glue perpendicular layers of wood boards together to form a dimensionally stable panel, is not new. The keystone dissertation by Gerhard Schickofer was published in Austria in 1994 and is often cited as the catalyst for subsequent CLT research and its application in modern-day construction [52, 56]. Today, the tallest mass timber building in the US, Ascent Tower in Milwaukee rises 25 stories (19 stories of timber over 6 stories of concrete) as a testament to the structural capabilities of the material. Using a simple post and beam system with large CLT floor panels [10], the building showcases the relatively unchanged rectilinear nature of CLT which is a product of historic wood milling practices of squaring logs into boards.

There are practical benefits to post and beam systems that may be materially inefficient but are easy to manufacture, transport, apply in multistory construction, and they behave in predictable ways under varying loading conditions[1]. However, as spans increase, these systems

require thicker beams which increase self-weight and the structurally underutilized material waste becomes a greater concern [1]. CLT is already considered a sustainable, efficient, and lightweight structural system [30], but there is an effort to further improve on these efficiencies. Recent studies from MIT have looked at reducing material in mass timber elements by removing lamella at CLT panel cores and digitally optimizing beam shapes and framing systems [39]. Others explore optimization for additive and subtractive approaches to remove excess material in both the core and at the surface of various engineered wood products [32, 34, 62]. Despite the material savings, there are few research examples exploring curved CLT panels. Zambrano-Jarmillo et al. developed a digital workflow to optimize both the material and structural efficiency of monoclastic CLT barrel vaults [66].

Structural optimization can be utilized in the design phase to leverage computational software to balance the often competing goals of shell design, such as reducing material volume while minimizing displacement [49]. Several studies explore digital structural analysis of shells while reducing material waste and evaluating parameters like the height to span ratio or shell thickness while seeking geometric diversity to reduce formal design restraints [13, 29, 49, 63]. Prior to the adoption of these programs, time-consuming and complex hand calculations were utilized to design shell structures [1]. Increasingly, designers are employing digital workflows, or an automation of tasks combining form finding, algorithms, and calculations, to facilitate the design process [20, 66]. This includes more recent adoption of machine learning (ML) and artificial intelligence (AI) models [20]. One literature review found an increase in use of surrogate-model-based multi-objective optimization using programs, like Opossum, in digital workflows to balance design objectives and unsupervised ML methods to distill complex data, aid in analysis, and visualize solutions. However, the author discusses how ML shows promise in early design phases for its ability to perform rapid iterations and complicated evaluations, but highlights the need for data expertise to make the method more accessible [20]. Employing these digital optimizations and workflow design tools could aid in finding a materially efficient double-curved form for CLT panels, but careful consideration must be made for manufacturing capabilities when designing thin shells [6, 13, 49]

1.4.4 Manufacturing

CLT in general is mostly produced as made to order, mass custom parts for large scale projects, which can increase the cost of production [8, 42]. This problem is amplified further when curvature is added to the equation. Bending wood can require custom molds or forms, additional equipment, or plasticization processing with heat, pressure or chemicals to achieve a certain radius [59]. An increasingly modernized and automated manufacturing system has made these more complex scenarios more efficient and economical [50]. Plasticization, however, can have a negative impact on wood's structural performance by damaging lignin and reducing the modulus of elasticity in exchange for greater bending [3, 9]. Cold molding is a well-established practice for curving wood laminates that bends untreated boards to a curved form and locks it in place with an adhesive without heat, pre-compression, or additional equipment to steam [59]. Benefits of cold molding are reduced stress to wood fibers and less hygroscopic motion from changes to moisture content, and it can be made cheaper by using wooden CNC'd molds rather than metal dies [25, 41]. Additionally, smaller radii can be achieved without plasticization if lamella thickness is reduced.

There are several studies exploring the incorporation of curved wood into manufacturing practices [43, 46, 59, 67]. Despite the improvements in curving processes, several studies critique curved wood products in research that are not feasible outside of controlled lab settings and use manufacturing considerations in their digital workflows, as well as a metric to test project viability [5, 6, 60, 66]. Synclastic CLT panels were researched and successfully fabricated in a 2015 project by Tannert et al. using thin 1" lamella cold molded over a wooden form. However, the use of 4" wide lamella required custom CNC geometry to create barrel shaped slats to reduce edge gaps [61]. However elegant this solution is, using narrow lamella from SDT could reduce the size of gaps between slats as well as reduce time and resources needed in board preparation.

1.4.5 State of the Art

Several reviews and studies have already been conducted globally looking for uses or testing the properties of wood from SDT [15, 18, 21]. One study experimented using low quality, underutilized hardwood boards that would not pass visual grading standards but, when subjected to destructive testing, met European strength requirements once they were incorporated into a

glue laminated beam [37]. Curved wood using various bending methods have been explored for material and mechanical properties for both boards [9, 19, 59] and engineered wood panels [3, 55, 58, 66]. Many explorations have tested timber thin shells for various improvements in mechanical, structural, or carbon reduction benefits [14, 51, 61]. However, there is a research gap of using wood from SDT in curved wood laminate panels.

Designers are increasingly able to perform more complex initial design structural shell analysis with Grasshopper components like Karamba. Recently, Musaab Mahjoub released an open-source beta website that allows for simple CLT plate analysis on Awatif.co [38] signaling a trend towards improved accessibility to engineering tools early in the design phase. This access is reflected in recent studies that have conducted digital structural optimization of curved CLT structures for architectural applications testing various parameters [23, 66]. Combining digital multi- objective optimization (MOO) with SDT species specific wood properties and fabrication checks could help bridge the gap between design, material sources, and manufacturing.

Several examples of curved wood being used in permanent architectural applications have been built over the years. Holzbau Unterrainer has developed a method for curving thick CLT structural panels used in several of their projects [28]. Urbach Tower by Stuttgart ICD/ITKE uses self-curving techniques to create thin CLT panel walls [5]. The Takeshige Yamashita Office designed a thin shell roof, curved in place, using LVL in the Toranoko Nursery project [69]. Elephant House at Zoo Zurich by Markus Schietsch Architekten uses four-ply CLT with two layers of lamella rotated to allow for panels to be bent in place aggregating into a large domelike structure [71, 75]. Additionally, several research projects explore optimizing curved CLT panels for various geometric configurations and fabrication parameters [23, 61, 66]. This thesis explores cold molding as the curving technique and looks specifically at double curved geometry that is prefabricated and transported to the build site.

1.5 Research Question

With the projection of demand for wood production, timber from SDT is a fiber source that can help meet demand, but material efficiency is still a vital consideration. As architectural designers, structures can be fine-tuned to further improve on material efficiency. This thesis asks if it's possible to leverage curved geometry to increase the material efficiency of CLT. Thin and narrow boards milled from SDT, especially when used in diagonal layup, are proposed as a

material source capable of creating efficient thin shell CLT ceiling panels. The primary objective of this thesis is to create a digital workflow that incorporates multi-objective optimization (MOO) geometry, wood -specific fabrication ability checks, and initial design structural analysis.

This initial research question is divided into two more targeted research questions.

1.) How can synclastic and anticlastic curved geometry be used to optimize material and structural performance in long-span CLT panels?
2.) How can CLT design and fabrication methods respond to and enable the use of low value fiber, or “thins” and “narrows”, from SDT?

CHAPTER II
GOALS AND OBJECTIVES

2.1 GOALS AND OBJECTIVES

Investigation into whether the dimensional properties of low-value "thins" and "narrows" from SDT can be leveraged in the design of lightweight, long-span mass timber structures is the primary goal of this thesis. Taking advantage of the inherent thin and narrow profile, which is a product of existing SDT milling practices, this research looks at an underutilized fiber source for its increased ability to bend and twist into double curved forms. Seeking to develop a long-span, thin-shell CLT panel, this study uses geometric optimization to achieve that span with substantially less wood than a typical rectilinear mass timber system. To pursue this goal, a digital workflow is developed that integrates parametric geometry generation, multi-objective optimization, initial design-phase structural analysis, and fiber source-specific fabrication checks. To evaluate this goal, the study establishes the following objectives:

1.) Optimize material and structural performance by evaluating iterated panel configurations for volume and meeting maximum allowable displacement standards.
2.) Evaluate geometry compatibility with proposed SDT fiber source by testing them against dimensional and material properties of thin and narrow Douglas fir lamella.
3.) Physically evaluate manufacturability through full scale prototyping using thin and narrow lamella and the proposed diagonal CLT layup
4.) Quantify potential material savings by applying selected geometry to a hypothetical long-span design scenario and comparing its volume with a conventional one-way post and beam mass timber system.

A tension exists between the two material goals of this project: the need to find high-value product applications for the large quantities of low-value fiber, and this project's goal to minimize material volume. This project does not seek to maximize the volume of low-value fiber through these long-span panels. Instead, it seeks a new market application where the curved geometry and span are not suitable for conventional rectilinear CLT or lamella dimensions, potentially increasing demand for the low-value fiber. The study does not, however, conduct an economic analysis of different product streams for fiber from SDT. Instead, it explores one potential pathway in which the characteristics of an underutilized fiber source are treated as a design opportunity while maintaining material efficiency as a fundamental objective.

CHAPTER III

MATERIALS AND METHODS

3.1 General Methodology

This study is divided into four sections: 1.) digital workflow development and multi-objective optimization, 2.) a long-span application design case study, 3.) material-specific fabrication feasibility checks, and 4.) physical prototyping and fabrication. The majority of the study is focused on a quantitative study of geometric, material and structural performance conducted with Rhino and Grasshopper. Throughout this workflow, the dimensional characteristics of "thins" and "narrows" from SDT were treated as material inputs that informed geometric, structural, and fabrication decisions rather than as a material substitution applied after geometry selection.

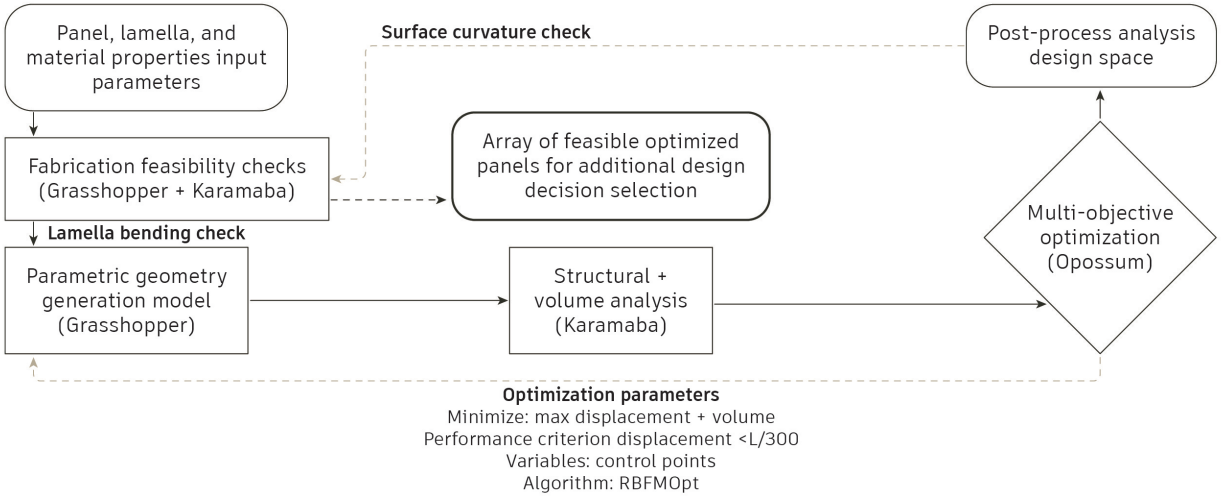


Figure 7. Digital workflow general methods

Section one (3.2) is the development of the parametric workflow which integrates geometry generation, MOO using Opossum, initial design structural analysis using Karamba, and statistical analysis of the MOO results (Figure 7). The second section (3.3) tests the post-process analysis portion of the workflow, by applying it in a hypothetical long-span CLT ceiling system to evaluate geometry configurations with defined dimensional, structural, material, and fabrication constraints. Section three (3.4) performs fabrication feasibility checks through fiber-source-specific material properties in a lamella bending analysis and panel surface curvature

evaluations. For the final section (3.5) of the study, manufacturability assumptions from the digital workflow are evaluated through fabrication of physical panel prototypes.

Using the competing objectives of minimizing volume and maximum displacement to evaluate performance, all optimization runs iterate 300 different geometry configurations using the algorithm RBFMOpt. Inputs for optimization are the Z-heights of control points which determine the curvature behavior of a geometry generation model. Each iteration represents a unique geometry. Karamba is used to test maximum displacement, and certain universal settings were used throughout all testing series. Figure 8 depicts the location of the distributed roof load and point supports used during testing. Additionally, a maximum allowable displacement value of L/300 [76], or 8cm, was used. Material properties were simplified to GL36h due to current limitations with Karamba.

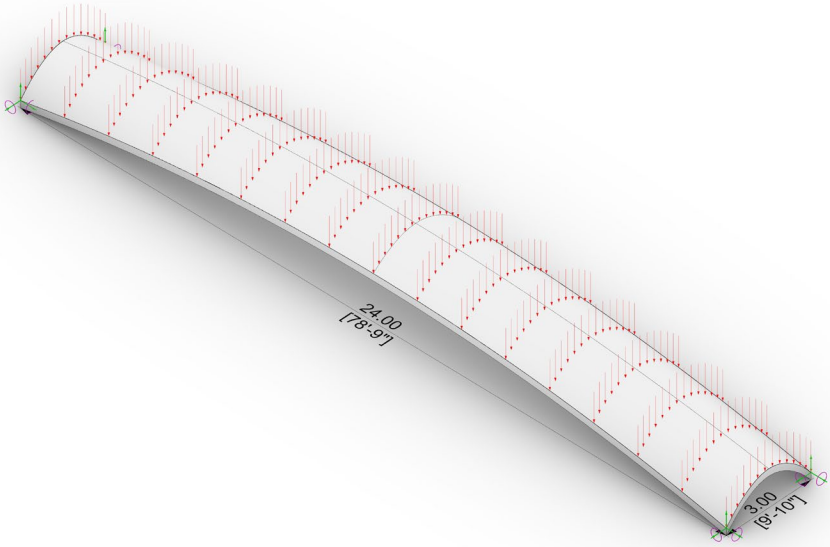


Figure 8. Karamba configuration: depicts how structural models are set up for all subsequent optimizations

For the long-span case study, a hypothetical design scenario was created to identify a geometry for curved CLT panels for the Eugene Airport concourse expansion. The concourse is planned to be 110’ wide and is well suited for the application of a shell roof structure as it is a long-span single-story building [54]. With the manufacturing of panels explored as being prefabricated off-site, panel dimensions of 3 m x 24 m were determined by transportation limitations. Using a selected portion of a panel identified through digital analysis, a 1:1 prototype

was fabricated for analysis of the manufacturability. This case-study forms the basis of the development of this framework as described in the following sections.

OpenAI's ChatGPT was used throughout the development of the computational workflow as an iterative coding and troubleshooting assistant. The use of generative AI supported the implementation of custom computational and machine-learning methods that otherwise require specialized programming and data-management skills. ChatGPT assisted with the development and refinement of Python scripts used within Grasshopper for data organization, Pareto analysis, k-means clustering, solution-space evaluation, and visualization. The author defined the analytical methodology, inputs, evaluation criteria, and interpretation of results, and all generated scripts were tested and iteratively evaluated within the Grasshopper workflow. In this capacity, ChatGPT was used to support the translation of author-defined analytical methods into executable code rather than to independently determine the methods or research outcomes. ChatGPT was also used as an editorial tool during thesis preparation to assist with organization, clarity, and revision of author-written text. All research decisions, analysis, interpretation, and final written content were reviewed and approved by the author.

3.2 Geometry Generation and Parametric Model Selection

A framework was developed for parametric geometry generation that facilitated formal exploration of the shells while maintaining control over fabrication-specific limitations. Rather than imposing a single predetermined geometry, this framework established a process of refinement of a family of related geometric models that could be varied through a limited number of control parameters impacting both the transverse and longitudinal curvature. The use of “narrows” from SDT informed this approach as a narrower lamella can more readily accommodate changes in the transverse curvature due to its increased ability to twist.

This framework was evaluated in three sequential phases (Figure 9) with the goal of screening five geometry generation models down to one model for subsequent post-process analysis. Phase 1 conducted an initial screening of the models to test lamella thickness 2.54cm based on thickness used in a comparable thin-shell CLT study [61]. Using a refined design roof load, phase 2 tested a thinner 1.6cm lamella thickness to evaluate panel performance with the minimum allowed lamella thickness for CLT [74]. The final phase tested a series of panel height

reductions stemming from fabrication considerations that a reduced height would reduce the material needed to create panel molds.

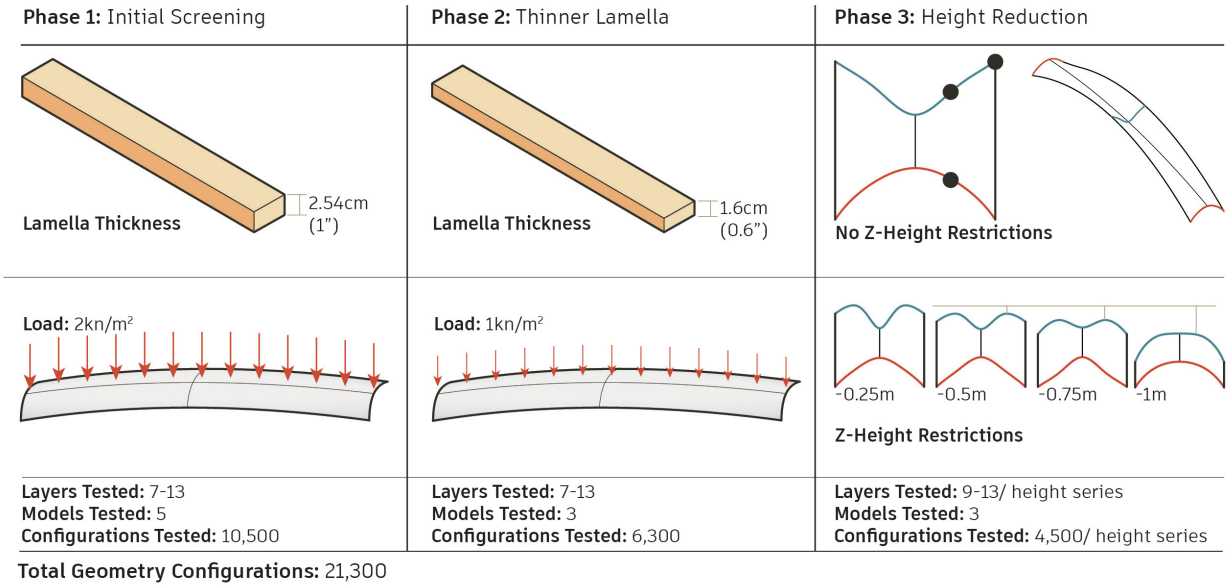


Figure 9. Geometry Model Screening Phases: describes each screening phase

3.2.1 Parametric Geometry Generation Framework

Developed in Grasshopper, the parametric geometry generation framework established a controlled approach for testing a range of shell geometry configuration. Designed to balance geometric variability with fabrication feasibility, the framework reduces the number of input variables while also reducing the potential for artificially restraining geometric possibilities. This is done by defining the panel through a control-point-based longitudinal spine and transverse rib system (Figure 10)

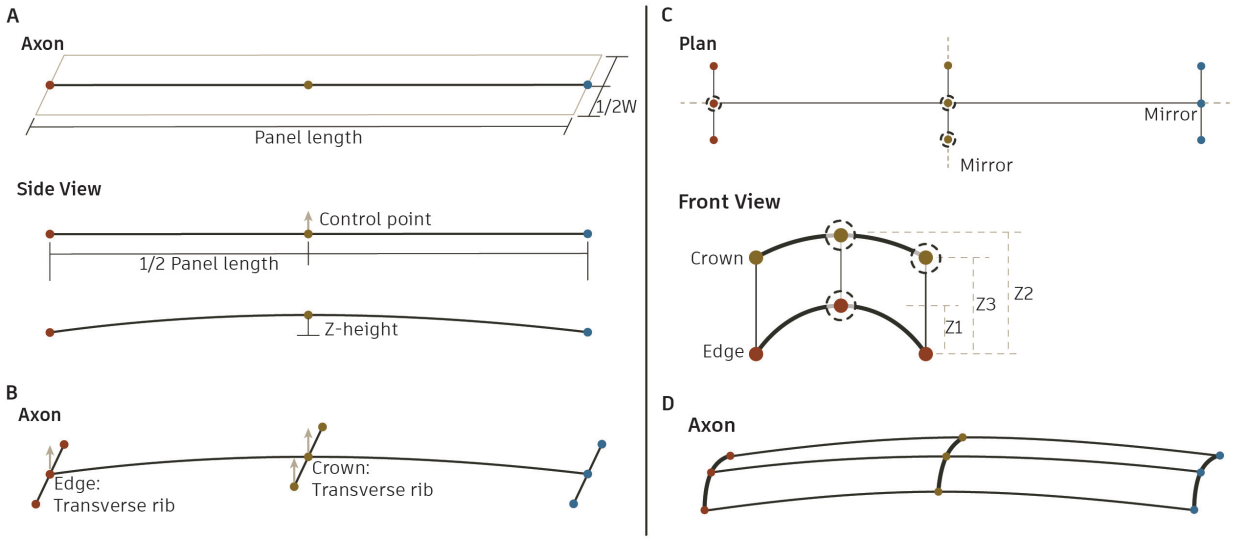


Figure 10. Parametric geometry creation process: A.) creation of transverse spine based on panel dimensions B.) creation of transverse ribs C.) symmetric parametric control points that move in the Z-direction D.) surface geometry curvature behavior controlled by moving the control points

Located at the center of the panel in the long direction, the longitudinal spine has a series of symmetrically distributed control points that define its profile. Transverse ribs extend perpendicular to the spine in both directions across the panel width. These ribs have additional control points which define the transverse curvature of the panel. All control points, except for fixed points at the corners for support boundary condition control, can be vertically translated parametrically. Finally, the surface is constructed using the rib curvature. Five geometry-generation models were developed in this framework that varied the number of transverse ribs and number of control points (Figure 11). The models tested were classified based on the number of ribs and rib control points as follows: three-rib/three-point (3R3P), three-rib/5-point (3R5P), five-rib/three-point (5R3P), five-rib/five-point (5R5P), and five-rib/five-point with a curved spine (5R5P-CS).

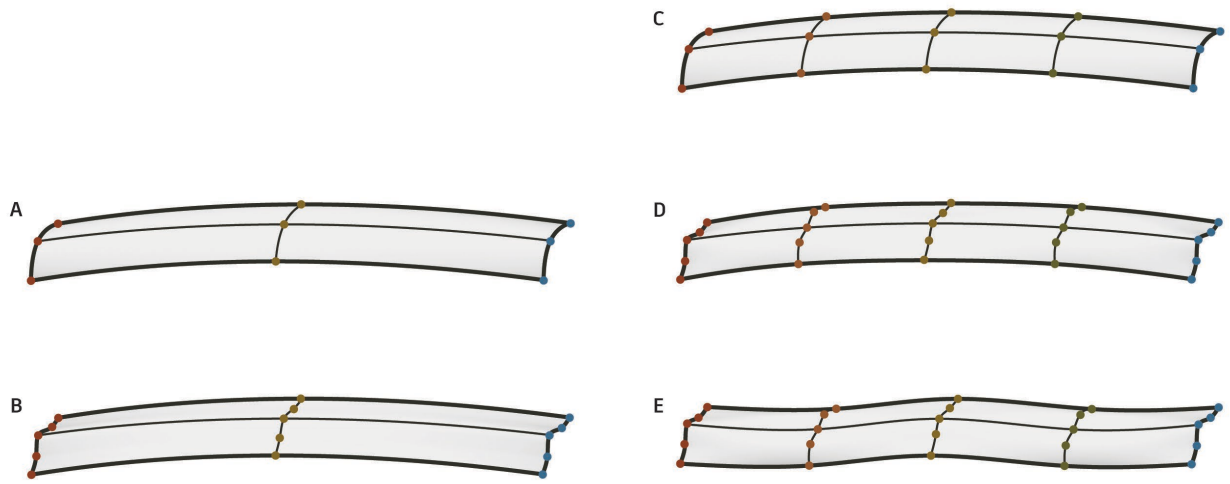


Figure 11. Geometry generation models: A.) three-rib, three-point or 3R3P model B.) three-rib, five-point or 3R5P C.) five-rib, three-point or 5R3P D.) five-rib, five-point or 5R5P E.) five-rib, five-point curved spine or 5R5P-CS

This classification of model parameters represents a progression of increasing complexity that introduced varying levels of geometric control. By increasing the number of ribs, an increased control of the panel's longitudinal curvature is gained, while increasing the number of rib control points more control of the panel's transverse curvature is gained. Increased control creates more formal flexibility resulting in a larger range of geometries for design consideration, but it also creates a potential for localized compound curvature incompatible with fabrication. The inverse is true for models with less parametric geometric control. Therefore, the subsequent model screening was constructed to determine the appropriate level of geometric control based on the model selection process

3.2.2 Geometry Model Screening

To evaluate the five parametric geometry generation models described in section 3.2.1. the three phases of the model selection process were conducted through a series of MOO studies. The goal of screening was to evaluate how different levels of parametric control affect material and structural performance, geometric variability, and fabrication complexity. This phase of study was not intended to identify a single optimized geometry configuration. Therefore, each model was subjected to a uniform optimization procedure resulting in a solution space that allowed for the comparison between the different geometry models. An individual 300-iteration

MOO was conducted for each ply count for each of the geometry-generation models tested within a phase.

Restricting the optimization inputs to adjust only model control points allowed for evaluation of geometry performance to be kept separate from panel thickness variables. With layer count being optimized separately, datasets resulting from MOO series were also kept separate during comparative analysis. Opossum automatically ranks configurations and initial results were screened based on a panel configuration's rank. Configurations within the highest rank were extracted and evaluated against the maximum displacement criteria of 8 cm. Solutions that met this structural performance criteria were retained as viable configurations for further analysis. Additionally, the number of viable configurations was recorded for each geometry model as a metric indicating frequency of displacement criteria satisfaction within the design space.

Material efficiency comparison was then conducted using both the minimum-volume viable geometry configuration and the distribution of volumes produced by panels within retained solution sets. As a broader indicator of model behavior, average volume was examined. However, due to the variation in number of viable configurations between the geometry models, average values were interpreted cautiously and not used independently to determine model selection. An additional consideration with volume is analysis in the number of panel layers. Increasing layer count increases panel thickness as well as complexity to fabricate for the CLT layup process observed during preliminary physical prototyping.

A qualitative layer of analysis was also conducted through visual inspection of a representative sample of geometry configurations from each optimization series. Samples were selected from the viable geometry configurations, including configurations with the minimum and maximum volumes, in addition to two intermediate volume solutions (Figure 12). The samples were compared by examining the range and complexity of forms produced by each geometry model prior to the development of quantitative curvature analysis described in later sections. Specific features looked for in the optimized configurations were if resultant geometries converged toward a limited geometric type and if the curvature across the panels surface appeared feasible to fabricate. This allowed for a visual evaluation of whether a model was producing a variable range of different geometries as to not restrict design possibilities while maintaining manufacturability in the panel's curvature behavior.

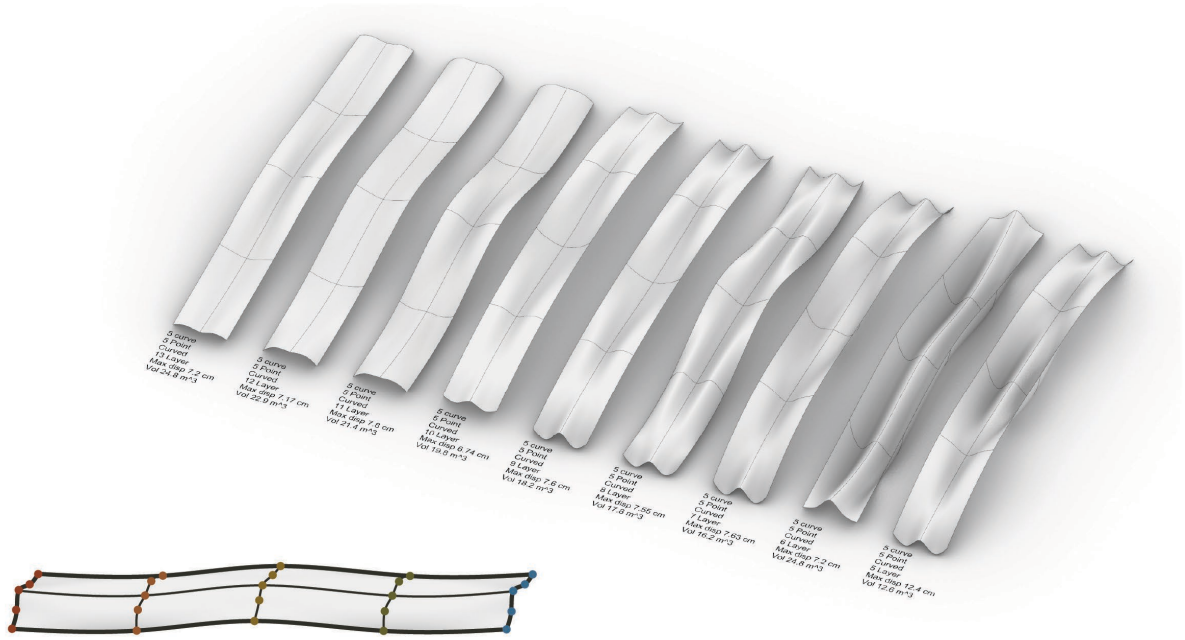


Figure 12. Visual comparison of layer series: 5R5P-CS geometry model minimum volume configurations for each layer series

Panels generated for phase 1 geometry screening used 2.54 cm thick lamellae and were subjected to a uniformly distributed load of 2kn/m^2. This load was intentionally conservative for phase 1 being twice the 1kn/m^2 design load utilized in long-span case study. Panel thickness was parametrically varied from seven (17.78 cm) to thirteen (33.02 cm) lamella layers or plies.

The goal of phase 2 was to reevaluate remaining geometry-generation models screened in phase 1, using material and loading assumptions more representative of those adopted for the subsequent long-span case study. Lamella thickness was reduced from 2.54 cm to 1.6 cm as the minimum allowable thickness per ANSI/APA PRG 320-2025 [74]. The uniformly distributed dead load was reduced from 2kN/m^2 to 1kN/m^2, this loading assumption followed the value employed for dead load in comparable curved mass timber study [24]. Panel thickness in phase 2 varied from seven (11.2 cm) to thirteen (20.8cm).

Phase 3 conducted a series of studies to investigate the effect of restricting overall panel height on structural performance. One fabrication constraint for these long span panels comes from the need for formwork in the cold mold lamination process. With increased panel height there would be an increased depth of mold which could be impractical to fabricate. By systemically introducing increasingly restrictive geometric bounds, phase 3 determines if the geometry models continue to produce structurally viable solutions within a reduced fabrication

envelope. Utilizing the same three models screened in phase 1, the layers tested for phase 3 were restricted starting at nine (14.4 cm) layers and testing up to thirteen (20.8 cm) based on phase 2 findings.

To reduce panel height, control points were progressively restrained by reducing the maximum allowable positive Z-Height. The specific control points that were restrained were points that contributed to transverse curvature above the longitudinal spine. Figure 13 shows on model 3R5P the corresponding points Z2, Z4, and Z5 that were constrained. Z-height restrictions were conducted in increments of 0.25 m after each complete MOO series. Preserving the underlying geometry generation logic, this approach facilitated the progressive restraining of the optimizer to produce tall panels.

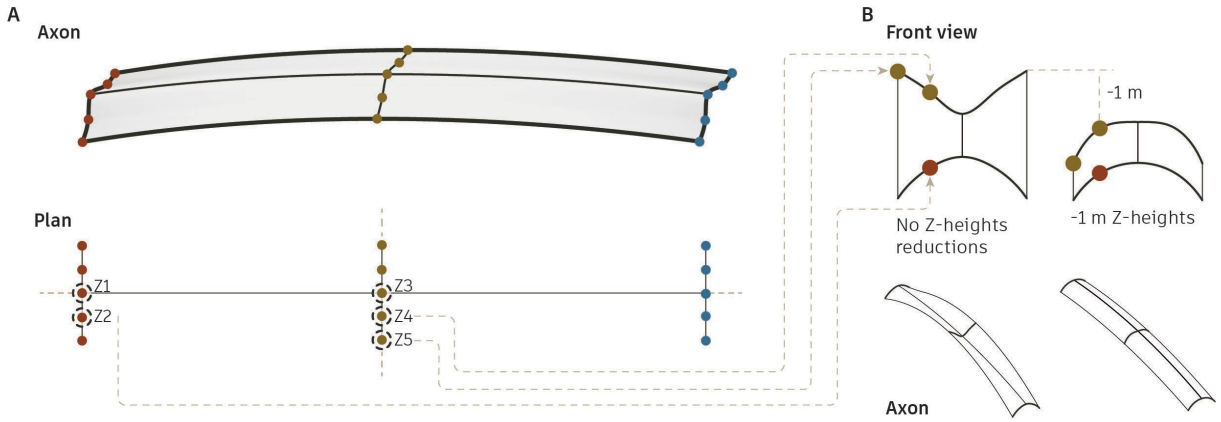


Figure 13. 3R5P geometry generation model: A.) axon of a 3R5P surface with all points B.) Z1-5 control points that are moveable in the Z-direction

3.3 Optimization Solution-Space Analysis

To further investigate the relationship between geometry, structural performance, and material use within the optimization solution space, a more detailed analysis was conducted targeted towards project specific needs. Continuing from the geometry generation and screening from section 3.2, a single geometry generation model was selected. Generated data logs from the phase 3 MOO series as detailed in section 3.2.2, were subjected to additional analysis including a Pareto and near-Pareto analysis, geometry-based k-means clustering, silhouette analysis, and visualization of the resulting geometric families and their performance characteristics.

3.3.1 Dataset Selection and Preparation

Selection of specific Z-height restriction data from phase 3 model screening was determined based on how it balanced reduced panel height, performance, and geometric diversity. Further narrowing down the data, three adjacent panel thicknesses were identified starting with the series that produces structurally viable configurations with the least number of layers. This provided three populations generated under equivalent geometric, material, loading, and optimization conditions. Each series contained 300 iterations resulting in a total of 900 configurations subjected to additional comparison. Maintained as separate populations, the layer series were evaluated independently of each other rather than by compiling all 900 iterations into one population.

For this more robust analysis, the entire data set of each layer series were evaluated instead of limiting it to high rank and structurally viable solutions. Opossum logs include objective values as well as the variable parametric values which control geometry. A custom ML Python component was developed within Grasshopper to extract and re-organize this data. Keeping a consistent data structure, iterations are assigned a number and kept grouped with their geometric variables for the control points (Figure 13) associated with the geometry model as well as the performance values. By maintaining a complete data set, evaluation could be done on all solutions, including those that performed poorly, for a more holistic understanding of the geometry within the design space. This organization facilitated subsequent performance and geometry-based analysis.

3.3.2 Pareto and Near-Pareto Analysis

Pareto analysis was used to evaluate the tradeoff between the two optimization objectives: minimizing panel volume and maximum structural displacement (Figure 14). Opossum's MOO identifies these tradeoffs for competing objectives based on a non-dominated solution Pareto front [65]. A solution is classified as Pareto-optimal when no other solutions within the optimization population produces an equal or lower value for both objectives while improving at least one. Therefore, the resulting Pareto front native to Opossum represents the set of non-dominated solutions defining the best observed tradeoffs between structural performance and material use.

For this phase of analysis, Pareto fronts were reconstructed independently from the logged layer series optimization populations during post-processing. Not intended to replace Opossum MOO analysis, this reconstruction is instead meant to provide a consistent analytical structure to visualize, classify, and compare complete solution populations with project specific analysis criteria. One such project specific criteria is the 8 cm maximum allowable displacement which was incorporated as a performance threshold and is represented as a line within the objective-space visualization. Rather than removing non-viable configurations, creating this threshold allowed for broader analysis of the whole population while having a readily distinguishable visual representation of configurations satisfying serviceability criterion.

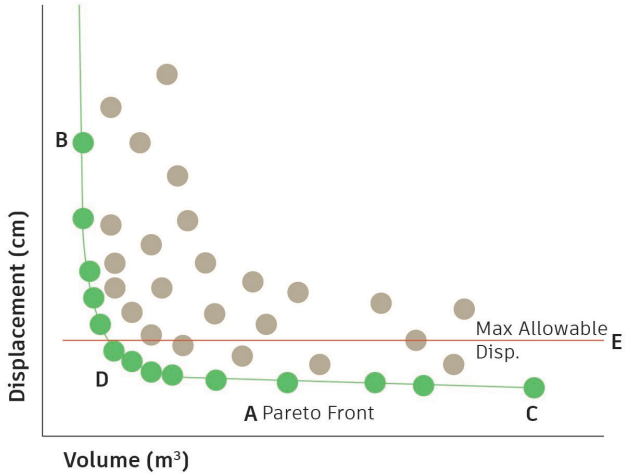


Figure 14. Diagram of Pareto analysis scatter plot: compares competing objectives volume vs. displacement A.) Pareto front is the line connecting all Pareto optimal solutions B.) area of front representing low volume but high displacement C.) area of front representing high volume and low displacement D.) area of the front where both objectives are balanced E.) max allowable displacement threshold line

Pareto classification alone, however, provides a binary distinction between non-dominated and dominated solutions without indicating proximity to the front for the remaining solutions. To add greater resolution within the dominated population, a near-Pareto analysis was added to post-processing. Calculating the relative proximity to the Pareto front, solutions were then classified using a tolerance-based system (Figure 15). A tolerance of 0.03 was utilized for this analysis. This creates a gradient distinguishing configurations that are located progressively further from the front which becomes an analysis metric for later geometric family comparison identified through clustering.

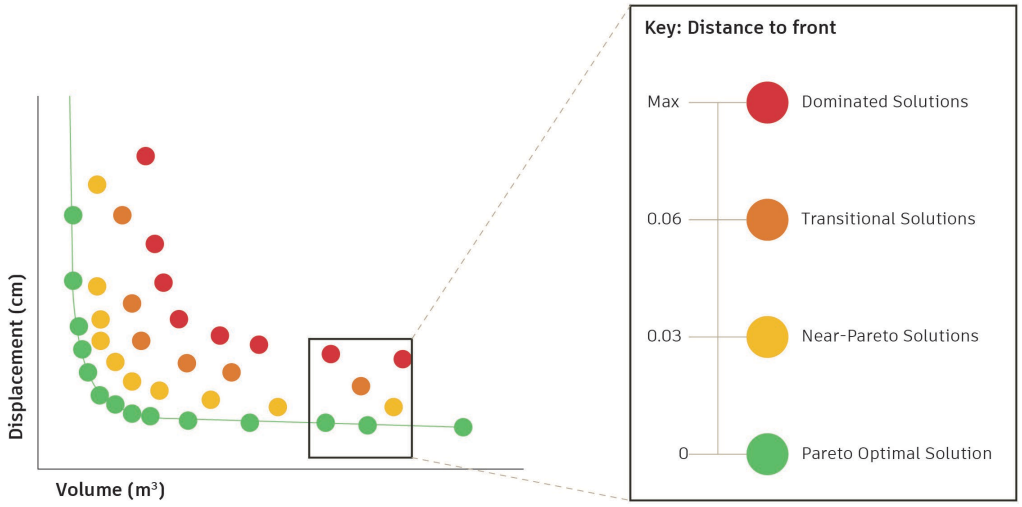


Figure 15. Diagram of near-Pareto analysis: depicts color gradient added to solutions outside of Pareto front based on their distance to the front

3.3.3 Geometry-Based K-Means Clustering and K Selection

Overlaid onto the Pareto scatter plot, a separate cluster analysis was developed to identify recurring geometric characteristics within the optimization populations (Figure 16). A k-means clustering acts to partition specific observations into a set number of clusters by minimizing variations around that cluster's centroid. Variations are evaluated by comparing the difference in the Z-heights of transverse ribs within a panel and comparing them to the Z-heights in other panels (Figure 17). The different panel configurations are then placed into a cluster and grouped based on similarities in their transverse ribs. Excluding volume and structural performance allowed for the isolation of geometric similarities for analysis.

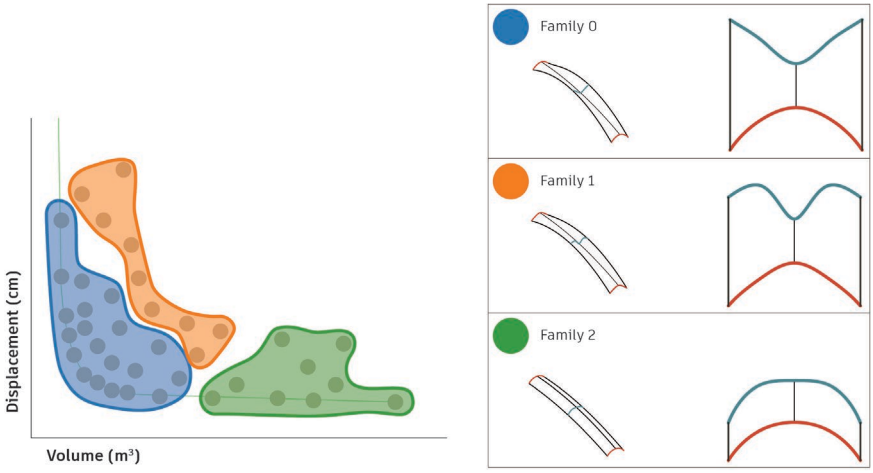


Figure 16. Diagram of k-means clustering: A.) cluster overlay on Pareto scatter plot B.) depicts how different clusters represent different recurring geometry configurations

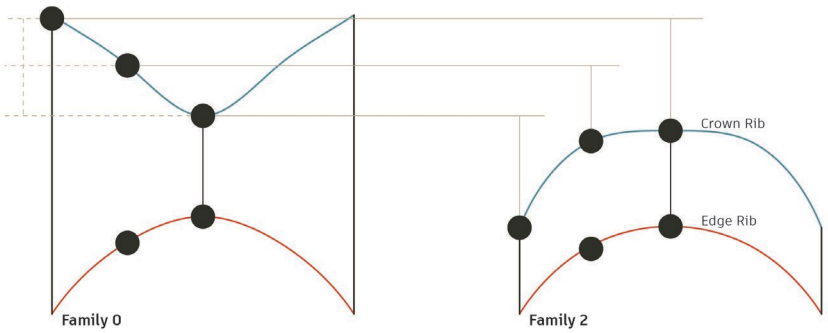


Figure 17. Cluster Z-height variation analysis diagram: depicts Z-height comparison of a panel's crown transverse rib in a family with the crown rib of a panel from a different family

The number of clusters in this analysis is determined by and equal to the k-value. Rather than pre-determining a k-value, multiple k-values (2-10) were tested and evaluated with a silhouette analysis. Incorporating this silhouette analysis test into the workflow allows for an automatic evaluation of selected number of clusters. The silhouette coefficient produced by this analysis compares the similarity of each solution to other members of its assigned cluster with its separation from the nearest neighboring cluster. Values approaching 1 indicate a comparatively well-separated cluster, values near 0 indicate overlap with neighboring clusters, and negative values indicate potentially ambiguous clusters. This average silhouette score provides a quantitative basis for selecting a clustering resolution appropriate to each geometric population evaluated.

Once the k-value was selected, each cluster was assigned an identification as a geometric family. The centroid of a cluster represents an individual geometry configuration with the mean control point Z-heights and is reconstructed to visualize a representative geometry for each family. Because this analysis compares three different layer series independently, identification labels of families do not represent equivalent geometric clusters between the two data sets (ex: family 2 in ten-layer analysis does not represent the same geometry in family 2 for the eleven-layer analysis). This allowed recurring geometric tendencies to be identified without predetermining geometry categories and provided the basis for subsequent geometry family comparison.

3.4 Material-Specific Fabrication Feasibility

Before optimizations were run, an initial fabrication feasibility check was conducted to evaluate whether lamella used in the panel could accommodate the geometric deformation

required during the cold-molding process without exceeding material capacity (Figure 18). Using species-specific material properties for Douglas fir [53], an orthotropic material model was defined in Karamba for a lamella with a thickness of 1.6 cm (0.6”) and width 2.8 cm (1.1”). These dimensions correspond with minimum allowable thickness and width standards for CLT per ANSI/APA PRG 320-2025 [74]. Using this minimum coincides with 1” boards milled from SDT that have an actual thickness of ¾” (1.9 cm) that, when planed for gluing surface preparation, would only need to remove 3 mm of material. For the width, 2.8 cm represents the worst-case scenario as the narrowest possible lamella instead of imposing a specific width, which can vary for boards milled from SDT [68].

Subjecting the lamella to a uniform load which is parametrically adjustable to the maximum vacuum pressure available during the cold-molding process and parametrically increased, the stress-to-strength ratio calculated by Karamba was monitored until the value was observed to approach 100%. The corresponding maximum displacement then provided an estimate of the maximum deformation the lamella could achieve before this threshold was exceeded. Comparing the maximum displacement with the maximum possible panel Z-height, a reasonable initial bound for geometry generation was established. Rather than defining a minimum bending radius, this analysis acts as a fiber-source aware design check that incorporates lamella dimensions and species-specific material properties into the geometric design space.

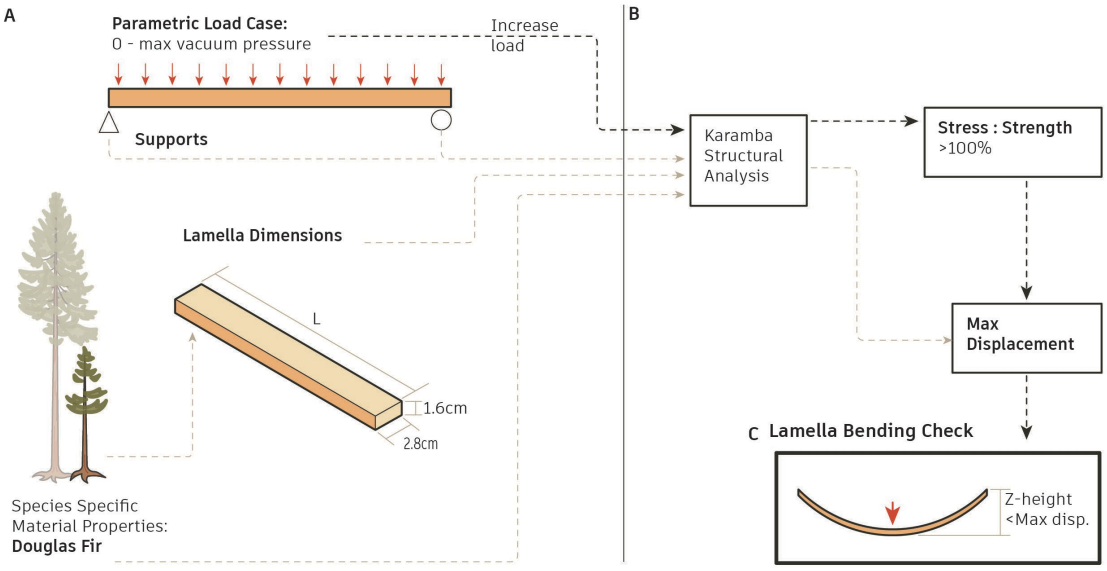


Figure 18. Lamella bending feasibility check process: A.) depicts the inputs used for the Karamba structural analysis B.) depicts the outputs relating to lamella bending C.) relates the max Z-height of a panel and the max displacement of lamella

Once the analysis described in 3.3 was completed, individual panels were selected as potential candidates for application in the long-span case study and subjected to an additional fabrication feasibility check. Surface curvature was evaluated for panels using Grasshopper's principal curvature component which characterizes both magnitude and direction of curvature. To simplify this analysis, the principal curvature in the longitudinal direction was used to evaluate surface curvature. The panel surface is discretized using a 64 x 16 evaluation grid, providing 1,024 mesh cells for curvature analysis. Curvature is evaluated in the transverse and longitudinal direction, allowing for areas of comparatively high and low curvature to be mapped to a panel's surface for visualization (Figure 19). The analysis returns curvature as C=1/R, where C is curvature and R is the corresponding radius. The bounds of the curvature values were extracted, and the maximum absolute curvature was used to determine the minimum corresponding radius, Rmin =1/|Cmax |. For fabrication screening, particular attention was given to longitudinal curvature due to the CLT layup used to produce the doubly curved panels. ANSI+117-2020 specifies minimum allowable curvature for glulam as 125 times the lamella thickness when the lamella thickness is less than 2.54 cm [70]. In the absence of a comparable U.S. standard addressing curved CLT, this criterion was adopted as a conservative reference and compared with the minimum longitudinal radius identified through the surface analysis.

These fabrication checks with optimization analysis were used to facilitate geometry selection for both the long-span case study and the 1:1 prototype.

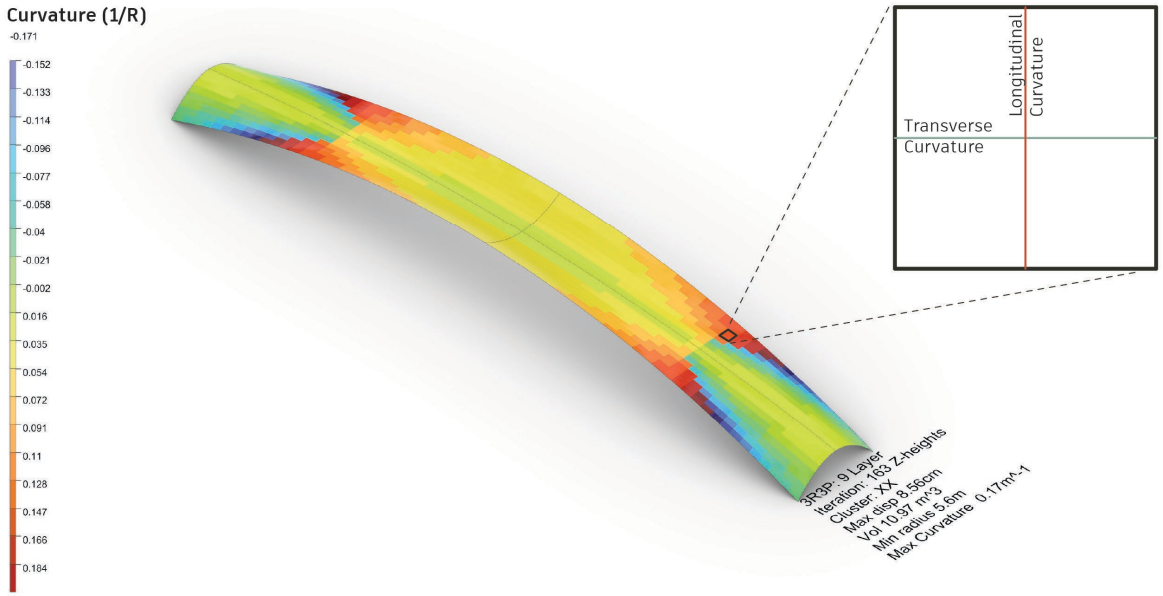


Figure 19. Curvature fabrication feasibility analysis: depicts evaluation grid on a panel with curvature mapped onto its surface and an example of how curvature is evaluated within a mesh cell

3.5 Prototyping and Fabrication

Prototyping was broken into two phases, a series of 1.) 1:4 scale prototypes were used to test lamination methods and layup approaches, and 2.) a 1:1 prototype to test the digital workflows fabrication checks. Results from the first phase of prototyping were used to inform processes for the 1:1 panel. Additional images documenting fabrication can be found in the appendix.

3.5.1 1:4 Scale Prototypes

1:4 scale models measured 1'x2' and used lamella dimensions of 6 mm x 20 mm or 2.4 cm x 8 cm at full scale. These dimensions were used as the thinnest and narrowest boards that could be safely processed at this scale and do not represent a true 1:4 scale of lamella used throughout the digital analysis of this study. Lamella were made by planning and cutting Douglas fir 2x4's into the 1:4 scale lamella. Figure 20 shows the different layup patterns tested. Layup option A was an initial test of feasibility for a standard DLT layup of two longitudinal layers on the exterior and two opposing diagonal layers at the center to balance internal forces. Layup B was to test if the panel could be balanced with fewer layers by dividing the center layer into 4 quadrants creating a X-configuration layup. A concave mold was created using wood 2x4's and was CNC'd into a simple synclastic form. Use of concave mold was tested to prevent some of the known problems with convex molds that pull vacuum bags underneath the lamination. PUR adhesive (Loctite HB X302) was used with membrane vacuum press with a maximum pressure of 21-25 inHg. Panels were pressed following manufacturer guidelines [36].

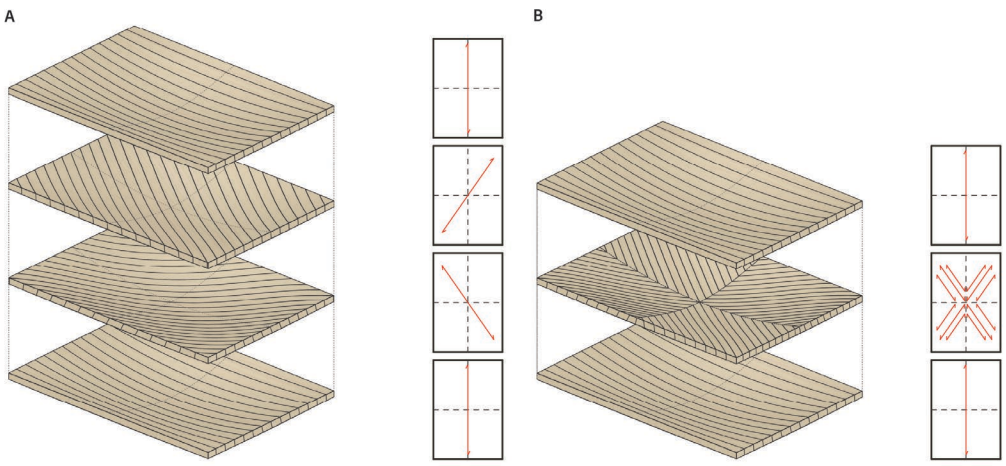


Figure 20. 1:4 scale prototype layup: A) four-layer DLT layup option B.) three-layer X-configuration layup option

Panels were evaluated for manufacturability based on tools needed to fabricate and the quality of lamination. Two panels were pressed with layup option A, and 1 panel was pressed with layup option B. Quality of laminations was assessed by an informal visual inspection of the laminated panel's edge off cuts checking for gap distances between face glue lines. Manufacturability was evaluated based on the ability of the panels to be fabricated using common tools already used in the CLT manufacturing process. Tools used for all panels fabricated include a CNC machine, table saw, chop saw, track saw, planer, and membrane vacuum.

3.5.2 1:1 Scale Prototype

The 1:1 scale prototype measured 2'x8' and used lamella dimensions of 1.6 cm x 2.8 cm based on the dimension used in the digital lamella bending feasibility check described in section 3.4. In addition to this prototype being used to evaluate manufacturability at full scale, it also provided a physical test of the proposed use of thin and narrows lamella dimensions of recoverable material from SDT. Lamella were produced by planning and cutting 1x4 Douglas fir boards into full-scale lamella. The same process was used to create a concave mold, the same PUR adhesive, minimum press time, and tools were used from the 1:4 scale model tests. Figure 21 depicts the layup of the 1:1 panel. Two vacuums were used to distribute pressure more evenly over the larger panel. Based on findings from the 1:4 scale model test, a wooden mold negative was cut for the center of the panel to pre-curve lamella layers and screw them into the mold after glue was applied. Removing the wooden negative before pressing, the panel was evaluated using

the same criteria as the 1:4 prototypes with the addition of analyzing the bending of full-scale lamella via lidar scan of physical geometry compared to digital mold geometry.

Digital CNC geometry was generated by taking the crown transverse rib curvature from the final long-span design case study panel. Taking a 2’ section from the middle, edge ribs were then created to form the surface geometry. Mold height was limited to 6” due to CNC height restrictions. This allowed for evaluation of the fabrication process with actual curvature found in the optimized panel.

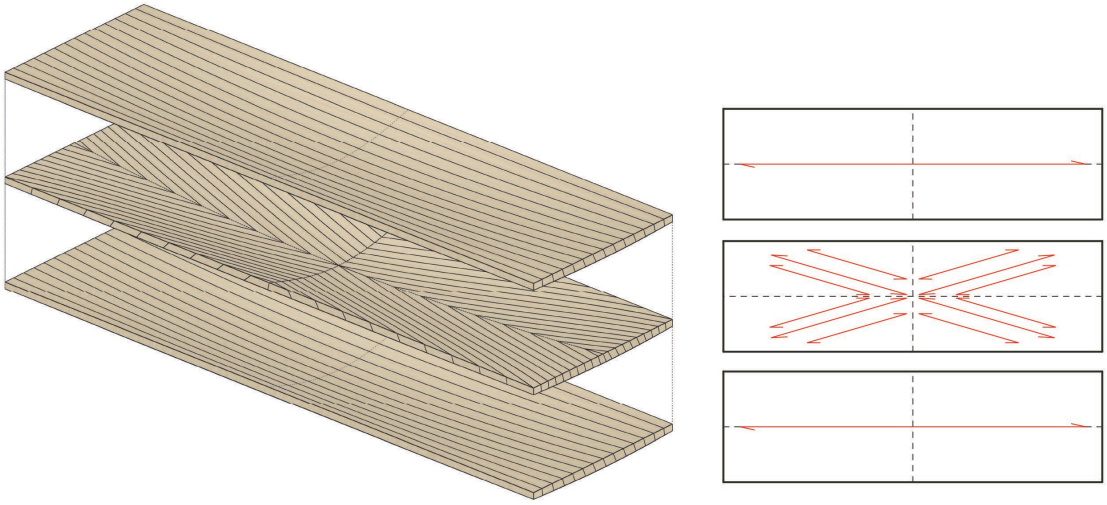


Figure 21. 1:1 scale prototype X-configuration layup

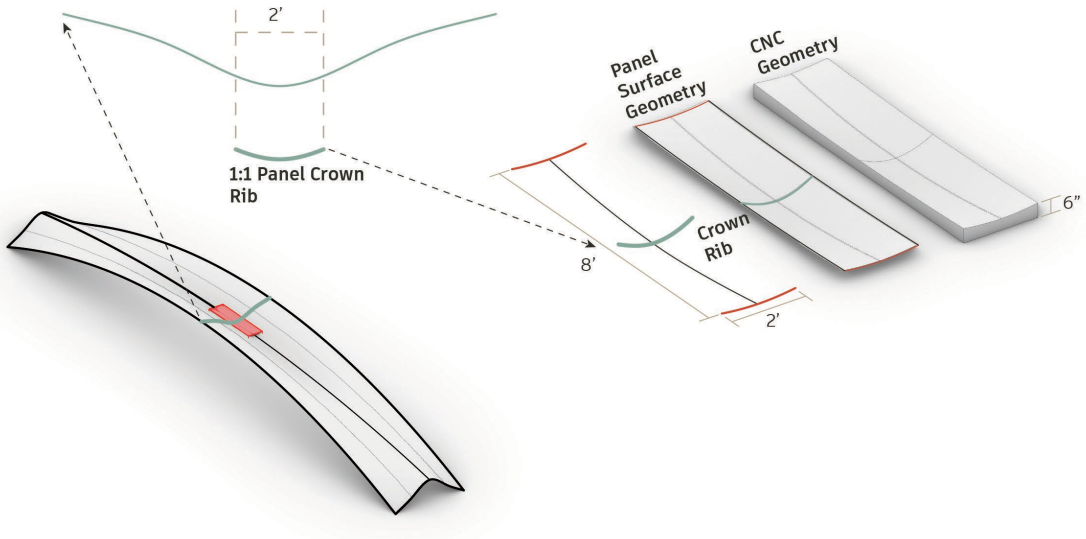


Figure 22. 1:1 panel geometry selection: depicts the process of creating CNC geometry for the panel mold from the long-span design case study

CHAPTER IV

RESULTS

4.1 Geometry Generation Model and Data Selection

Each phase of the geometry generation screening process led to findings that refined the methods applied the subsequent phases. Phase 1 found important relations between increasing number of control points and an increased range of geometric possibilities which contributed to increased curvature complexity. Eliminating the two most complex models, 5R5P and 5R5P-CS (Figure 23), due to visual evaluation of curvature being considered too excessive, phase 2 tested the three remaining models. For the second phase, reducing the lamella thickness had a predictable impact on performance with all models failing to produce a structurally feasible configuration in the seven and eight-layer series, and the 5R3P model failed to produce any until layer twelve. Because increasing layer count increases thickness, volume, and fabrication complexity, the 5R3P model was noted for its poor performance in phase 2. The three models were retained and tested during the height restriction series in phase 3, this time testing layer nine through thirteen based on phase 2 findings. Model 3R5P stood out as the only model to produce viable configurations after the first 0.25m reduction and continued to do so for all four-restriction series for a total of -1m in Z-Height restrictions.

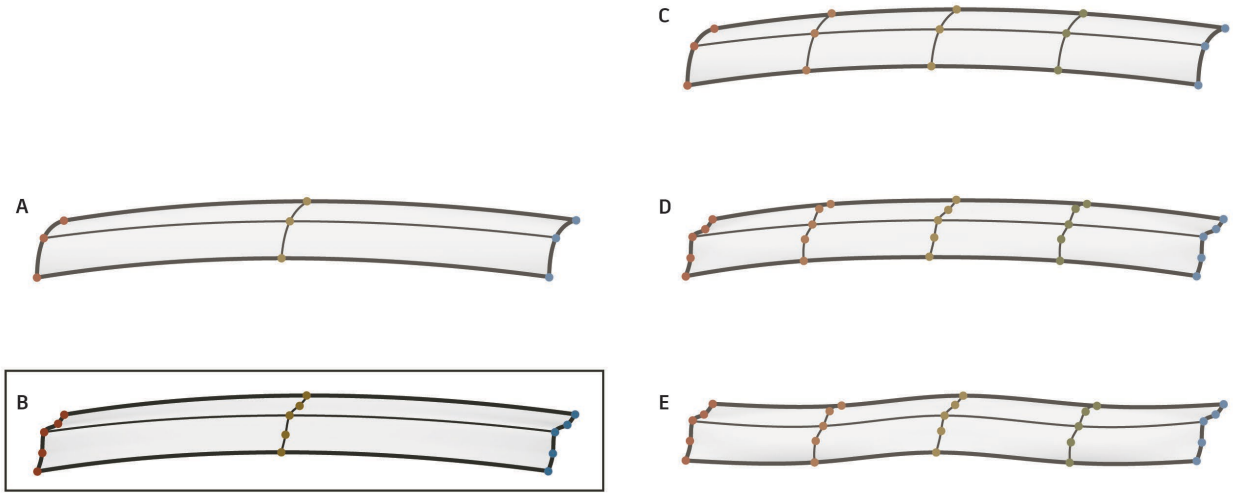


Figure 23. Final geometry model selection: A.) 3R3P B.) selected model 3R5P C.) 5R3P D.)5R5P E.) 5R5P-CS

The 3R5P was identified as the geometry generation model used for the long-span case study and subjected to the post process analysis. In addition to its ability to produce feasible configurations under increasing height restrictions, it consistently produced a balance of

competitive low-volume solutions, a higher number of viable configurations, and provided an increased range of geometric forms in all three screening phases. For data selection for post-process analysis, the height restriction series of -0.25m was selected for balancing height reduction with volume and providing the largest population of feasible configurations. From the -0.25m optimizations, layer nine was identified as the series that produced feasible configurations for the least number of layers and was selected, along with the adjacent ten- and eleven-layer series, for additional analysis. Figure 24 depicts this process and conveys panel thickness as well as the number of configurations evaluated in subsequent analysis.

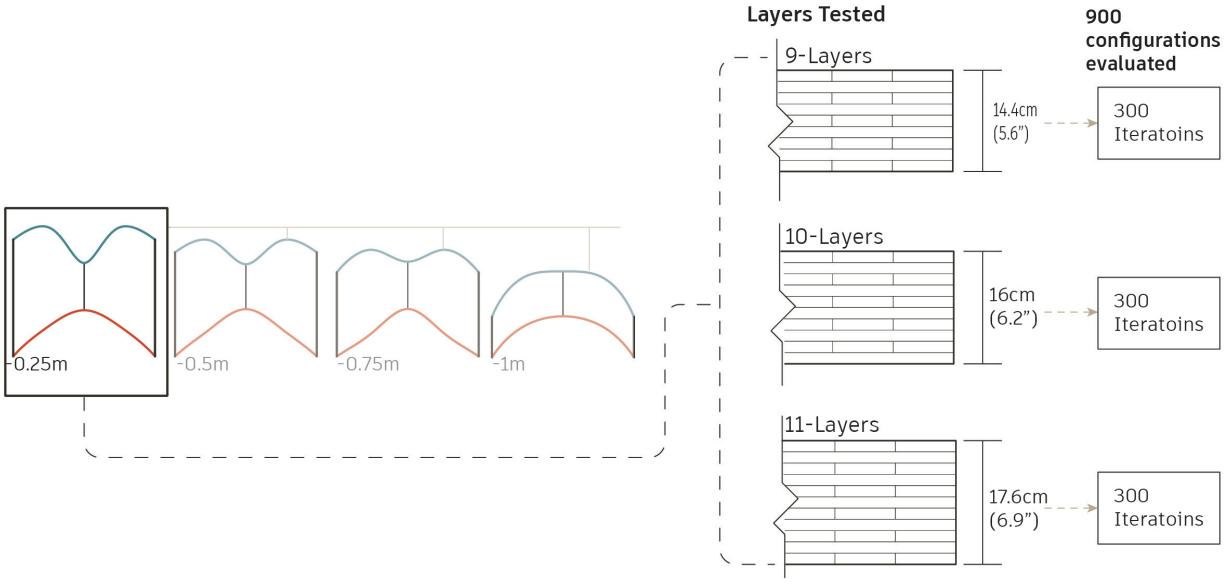


Figure 24. Data selection diagram: depicts the height restriction and layer series chosen for post-process analysis as well as the number of configurations evaluated

4.2 Long-Span Application Case Study

4.2.1 Multi-Objective Performance of the Nine Through Eleven-layer Panels

The MOO evaluating the relationship between displacement and material volume for the nine through eleven-layer series described in section 3.3 allowed for the comparison of the populations in terms of Pareto optimality, proximity to the Pareto front, and compliance with max allowable displacement of 8 cm. Table 1 summarizes the optimization results for each of the three MOO layer series.

Metric	9 layers	10 layers	11 layers
Solutions	300	300	300
Pareto-optimal	**66**	58	46
Pareto %	**22.00%**	19.33%	15.33%
Near-Pareto, tol. 0.03	120	150	**230**
Feasible ≤ 8 cm	108	**147**	86
Feasible Pareto	**37**	35	16
Best feasible displacement	7.9808 cm	**7.7550 cm**	7.9070 cm
Best feasible volume	**10.9417 m³**	12.0539 m³	13.1856 m³
Best feasible iteration	163	260	176

Table 1. MOO result comparison of the nine through eleven-layer series: Feasible solutions = max displacement ≤ 8 cm, near-Pareto solutions = normalized Pareto-distance tolerance of 0.03.

Producing the greatest number of Pareto optimal solutions of 66 out of 300 (22% of the series population), the 9-layer series generated 108 feasible configurations with 37 of these being Pareto-optimal (Figure 25). Increasing the panel to ten-layers changed the distribution, decreasing the Pareto-optimal solutions to 58 (19.3% of the series population) but also increasing the total number of feasible configurations to 147 (49% of the series population) (Figure 28). A different pattern emerges for the eleven-layer series that further decreased both the Pareto-optimal solutions to 46 (15.3% of the series population) and the total feasible configurations to 86. Further, when comparing solutions that are both feasible and Pareto-optimal, the eleven-layer series had a substantial decrease in solutions with just 16 compared to the 37 and 35 in the nine and ten-layer series respectively.

Considering additional metrics in the analysis produced further filters in the selection process. For example, the eleven-layer series had the largest number of near-Pareto solutions of 230 indicating that despite this reduction in strictly non-dominated solutions, much of this series design space remained relatively close to the optimized displacement-volume trade-off. The analysis also automatically highlights the iteration from each series that has the least volume in the feasibility range. When comparing the series, the nine-layer iteration 163 has the smallest

panel volume (10.9 m^3) of all three series. The ten-layer series had the smallest maximum displacement (7.75 cm) but came with an increase in material volume of about 10.16%.

Taken together, the results demonstrate that increasing panel thickness did not produce a simple monotonic improvement in optimization performance. Each layer series instead produced a distinct distribution of solutions: nine-layers with high material efficiency and Pareto-optimal feasible solutions, ten-layers with the largest total feasible solutions, and eleven-layers with the greatest concentration of near-Pareto solutions. These differences indicate that panel thickness influences not only structural capacity and material use, but also the distribution of high-performing geometries within the available design space. In the context of utilizing thins and narrows from SDT, this volume difference between layers is particularly important because reducing panel volume also reduces the total number of individual lamellae required to produce the panel. Therefore, material efficiency within the optimization represents not only a reduction in wood volume, but a more efficient application of the available SDT fiber resource. This distinction is important for subsequent analysis that, rather than identify the final geometry on performance or from Pareto membership alone, establishes metrics to further reduce population for further examination.

4.2.2 Geometry Family and Cluster Analysis

To examine whether recuring geometric characteristics were associated with optimization performance, K-means clustering was applied to each of the nine through eleven-layer series populations. Using silhouette analysis to determine the value of K resulted in different cluster numbers for each series: three for the nine-layer series (Figure 27), five for the ten-layer (Figure 29), and two for the 11-layer population. This indicates that increasing panel thickness did not reproduce the same organization of geometric differentiation, instead each population exhibited different degrees of differentiation. It should be noted that silhouette criterion should not be interpreted as identifying the definite number of shell geometry configurations. Because it evaluates similarity and separation between the control point height parameters, smaller cluster sizes can lead to families with slightly more geometric outliers.

The cluster analysis produces family galleries that allow for additional analysis of the representative shell for each family within each of the layer series depicting its transverse ribs and displaying mean performance data (Figure 26 and Figure 30). From the 9-layer series three

families, family 0 had 170 of 300 solutions with the highest silhouette score between the three of 0.491. With the largest K-value, the ten-layer series had five clusters with the dominant family being family 0 having 143 solutions and having the highest silhouette score of 0.544. Although the eleven-layer series dominant family was strong with a 98.3% Pareto or near-Pareto presence, its mean volume was the highest (13.95 m^3) of the three series confirming analysis from 4.2.1. Due to the added material volume contradicting efficient use of fiber from SDT goals, as well as the fabrication complications that come with increasing layer count such as the increase in lamella to produce, layup, and consolidate; the 11-layer panel was excluded from further analysis.

One interesting finding comes when comparing the nine-layer Pareto scatter (Figure 25) plot and its cluster analysis (Figure 27) overlay. The area representing the dominated solutions in red, the near solutions in yellow, and the Pareto-optimal in green aligns with family suggesting a relationship to geometry family and performance. This division is less clear in the ten-layer cluster analysis (Figure 29) with its increase in cluster numbers, where all clusters appear mixed except for one cluster concentrated along the Pareto front. For both the nine- and ten-layer series, this cluster on the Pareto front is represented by the dominant performing family identified as balancing low-volume, structurally feasible configurations, and having the most Pareto-optimal solutions.



Figure 25. Nine-layer series Pareto analysis: compares displacement vs. volume with color representing distance to Pareto front



Figure 26. Nine-Layer series family gallery: representative shells from the three different clusters, their transverse ribs, and important statistical information.

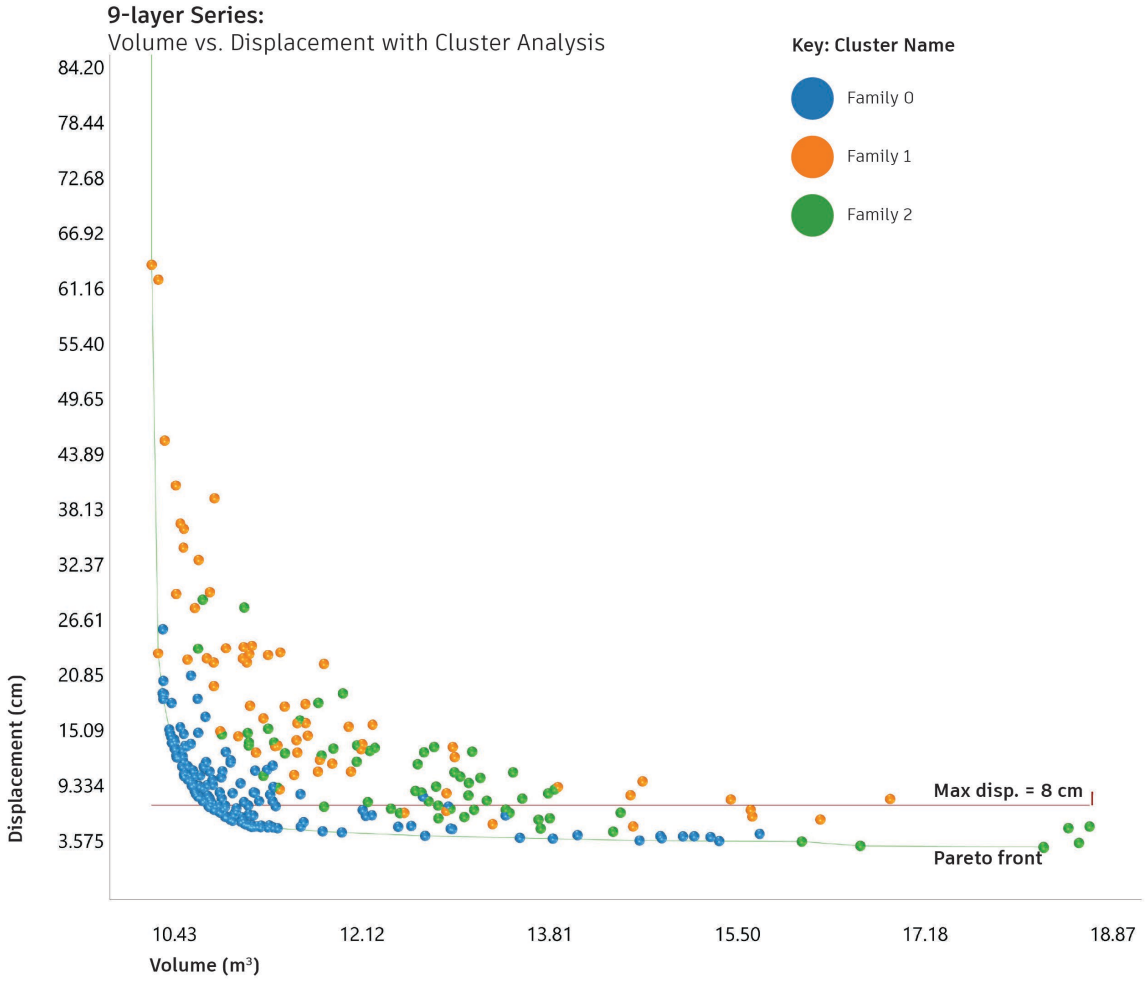


Figure 27. Nine-layer series cluster analysis graph: compares family cluster on top of Pareto scatter plot of displacement vs. volume

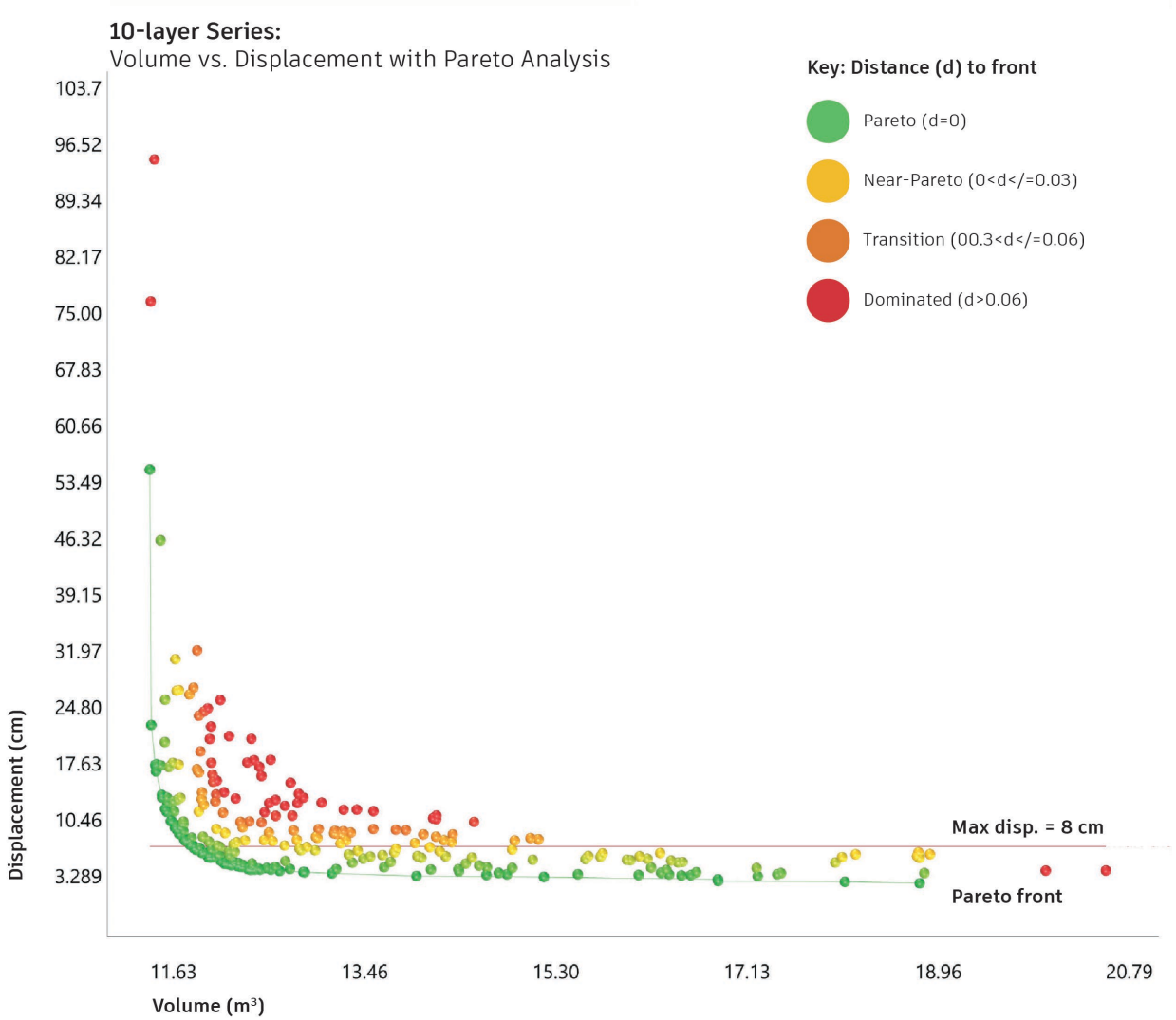


Figure 28. Ten-layer series Pareto analysis: compares displacement vs. volume with color representing distance to Pareto front

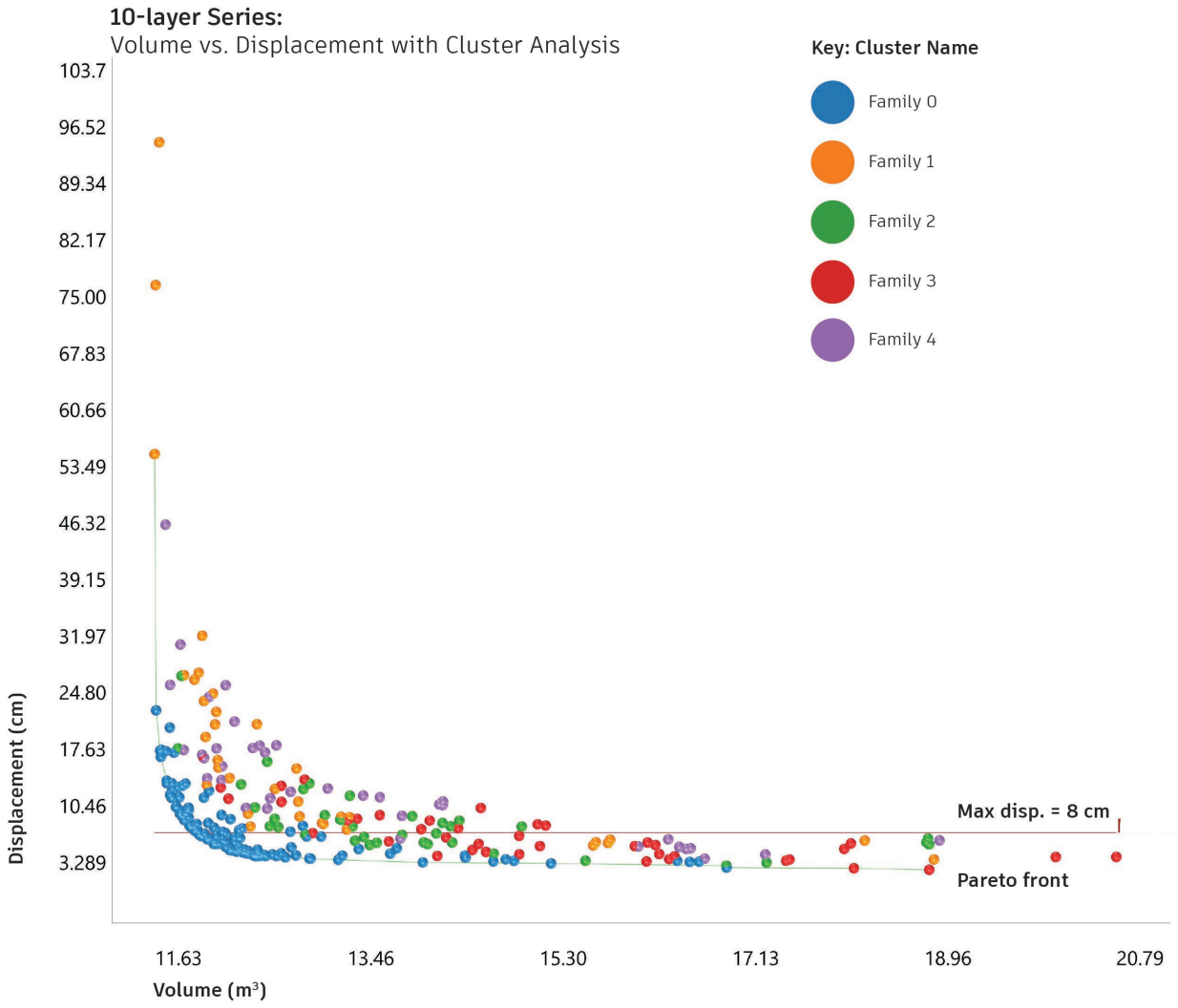


Figure 29. Ten-layer series cluster analysis graph: compares family cluster on top of Pareto scatter plot of displacement vs. volume

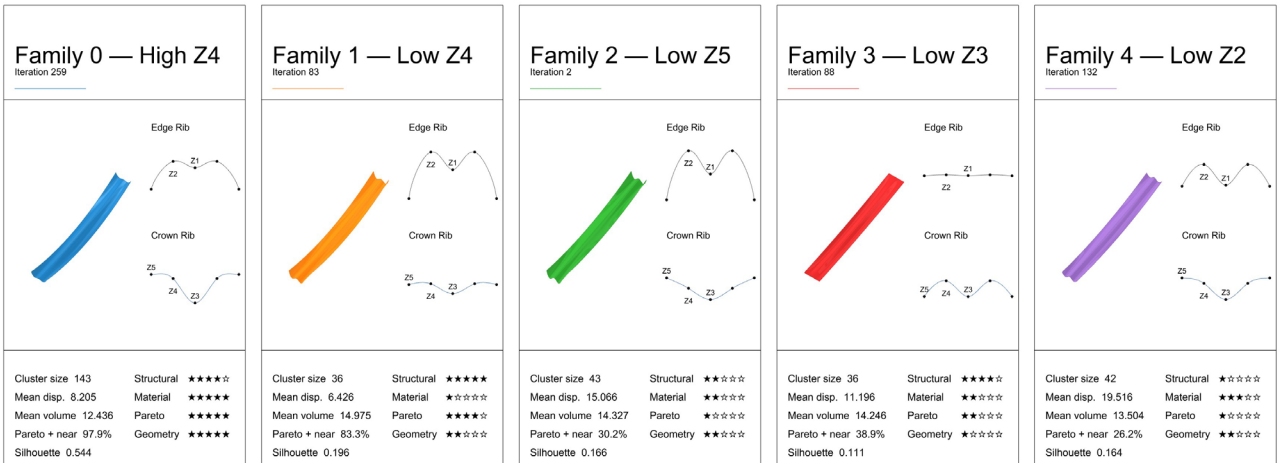


Figure 30. Ten-Layer series family gallery: representative shells from the five different clusters, their transverse ribs, and important statistical information.

A particular relationship emerged when comparing the dominant families from the remaining nine and ten-layer populations. Despite being clustered independently, family 0 from both series exhibit similar transverse curvature characteristics (Figure 31). This suggests that this geometry configuration represents a robust region of the geometric design space rather than an isolated result of a single optimization run. Further, by analyzing the mean performance and percentage of Pareto and near-Pareto between these two families finds a similar trade off to the analysis in 4.2.1. Increasing layers from nine to ten decreases mean displacement while increasing both mean volume and Pareto or near-Pareto solutions in the dominant geometry family.

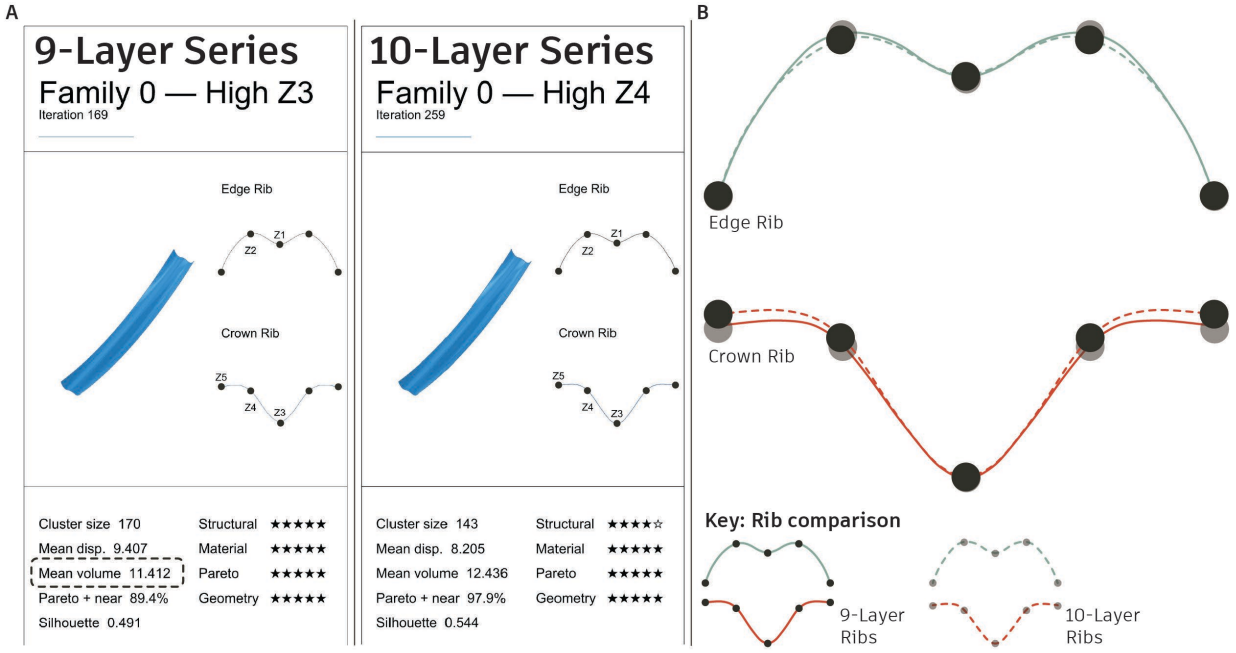


Figure 31. Dominant family comparison: A.) family 0 representative geometry highlighting the lower mean volume for the 9-layer series B.) compares the similarity in transverse rib geometry between the 9- and 10-layer series

Between these remaining populations, clustering results reinforce the advantages previously observed for the nine-layer series. Both the nine and ten-layer series produced dominant families with similar curvature profiles indicating that the favorable geometric behavior was not dependent on the additional tenth layer. The nine-layer series therefore demonstrated that favorable geometric behavior could be achieved with fewer layers and lower material volume, providing a more materially efficient application of “thins” and “narrows” from SDT.

4.2.3 Candidate Selection for Long-Span Application

Selection for final geometry was narrowed down further to the 36 solutions that were both feasible structurally and Pareto-optimal configurations from the nine-layer series family 0. Visual observation of this population found a few geometric outliers in the family that represent the outer edges of cluster's geometry (Figure 32). Additionally, these configurations had higher volume than others in the family and represent the high-volume end of the Pareto-front (Figure 33). The configuration from these outliers with the least volume, iteration 285, and the configuration identified as the best performing, iteration 163, by the ML custom python components were selected for additional analysis.

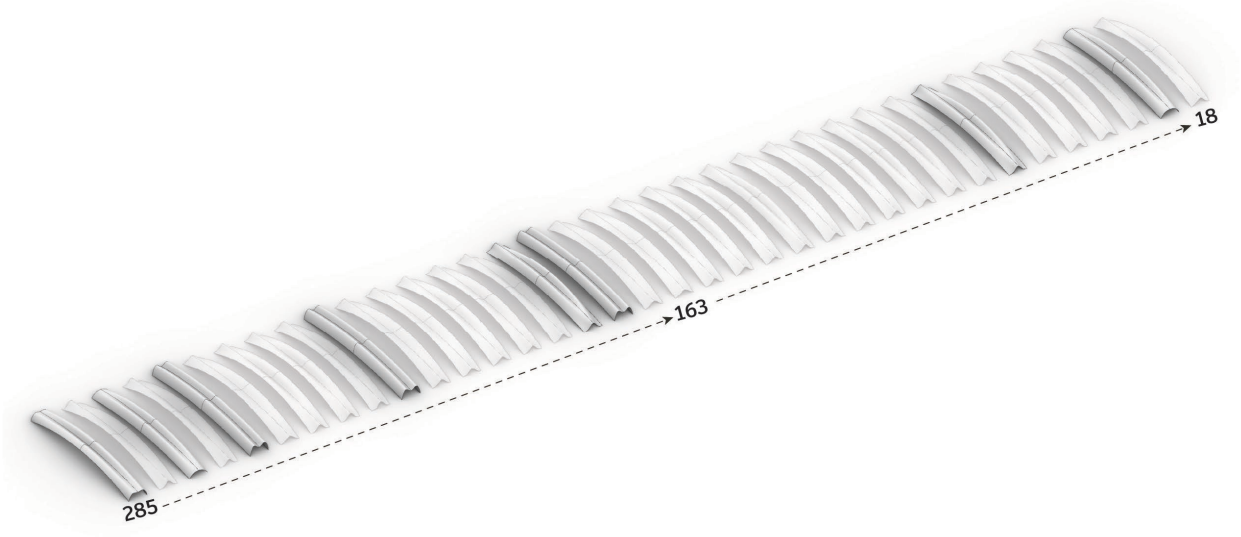


Figure 32. Geometric outliers: identified from the nine-layer series family 0 organized by iteration identification number

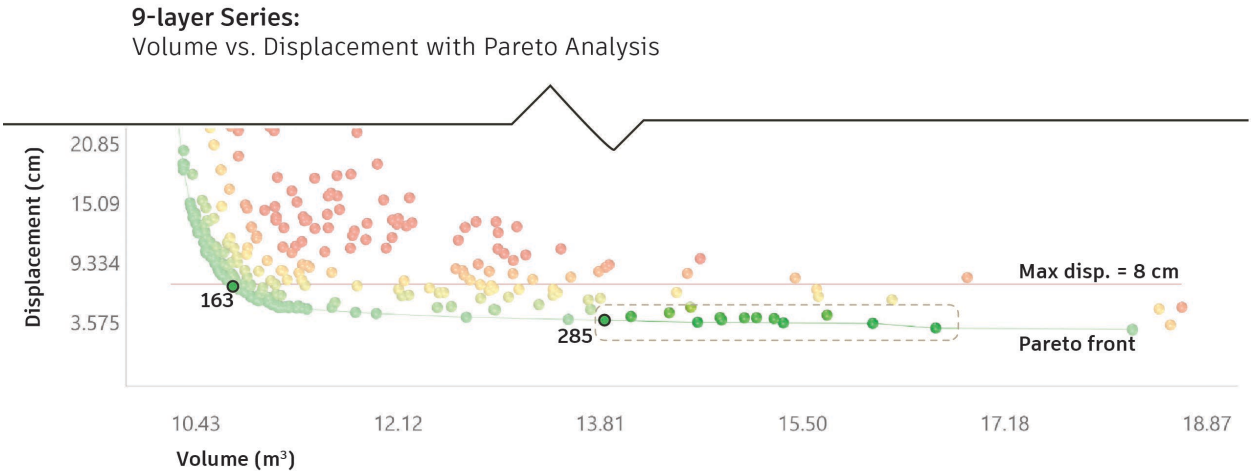


Figure 33. Iteration 163 and 285 on Pareto-front: locates the region of the Pareto front where geometric outliers can be found, iteration 285, and 163

Selected configurations within this population were then evaluated using the longitudinal curvature analysis described in section 3.4. This allowed for an additional metric to filter out configurations that were not feasible to fabricate despite meeting displacement and volume performance goals. For example, iteration 176 had a competitive volume but was found to have a minimum longitudinal radius less than the allowed minimum. When comparing 163 and 285 (Figure 34), both were within minimum allowed radius in the longitudinal direction with 285 having a minimum radius of 14 m or double 163 minimum radius of 7 m. However, this larger longitudinal radius came with a trade off with 285 having a more extreme transverse curvature that could introduce complications in the forming process even with diagonal layup of layers. Additionally, design decisions, such as detailing and construction considerations, were then applied by evaluating edge conditions and how panels would be joined when aggregated together. When aggregated, 163 displayed a more consistent relationship between adjacent panels when compared to other candidates (Figure 35), reducing anticipated complexity in the panel-to-panel detailing

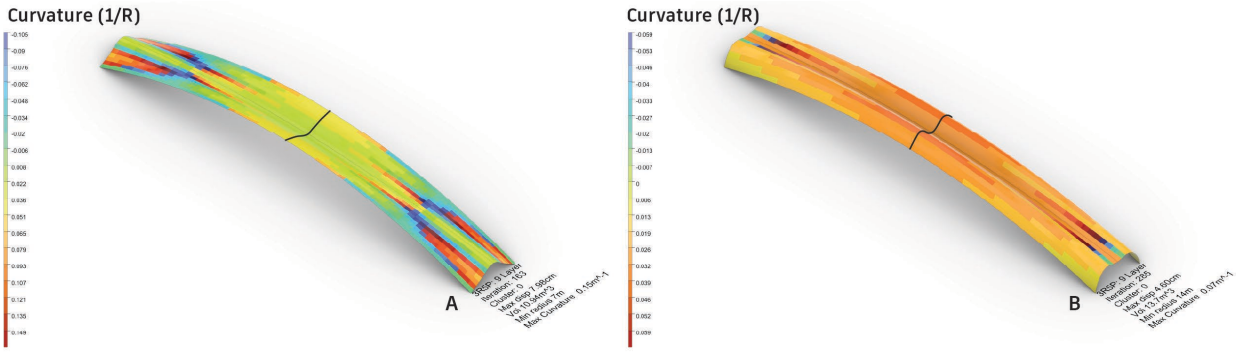


Figure 34. Curvature analysis comparison: depicts the visual mapping of curvature on panel surfaces A.) iteration 163 minimum radius 7 m B.) iteration 285 minimum radius 14 m

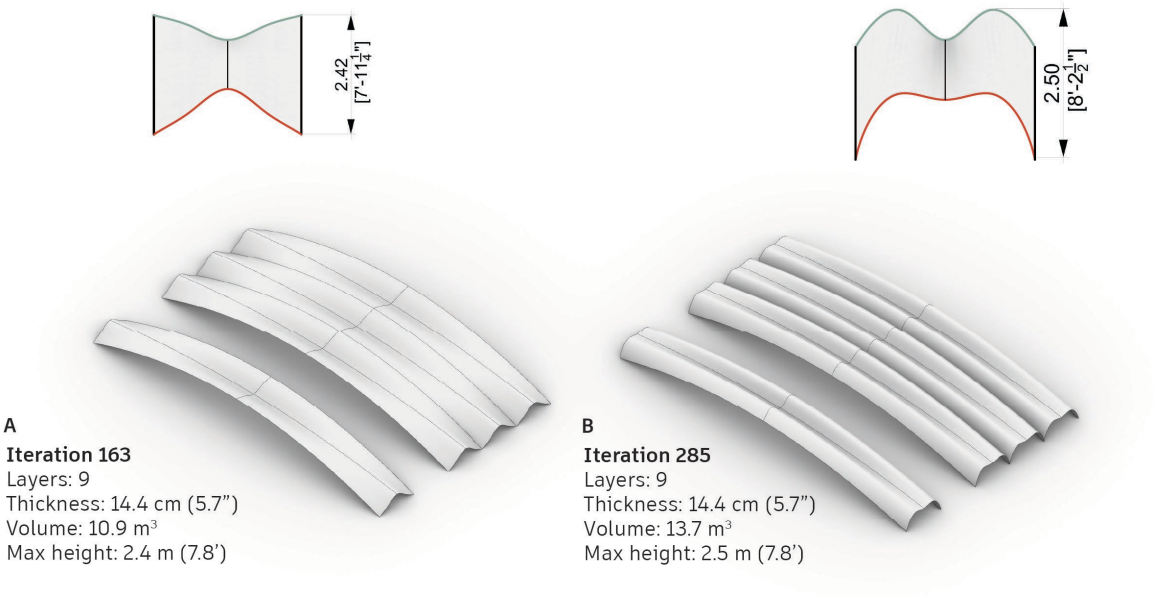


Figure 35. Edge condition comparison: compares the front view transverse rib configuration with an axon view of aggregated panels A.) iteration 163 B.) iteration 285

Iteration 163 was selected as the final geometry for use in the long span case study. It was identified as the best feasible solution within the Pareto analysis. Having a maximum displacement of 7.98 cm and a volume of 10.94 m^3, the panel also maintained a longitudinal minimum radius of 7.0 m. Importantly, these criteria also maintain the connection between geometric optimization and the proposed material source, as the selected configuration achieves its performance using the thin and narrow lamella dimensions established for SDT while remaining within the fabrication constraints associated with bending those members.

To examine the role of the geometry generation model, the z-height values from 163 were applied to the 3R3P geometry model. Despite 163 exhibiting an anticlastic geometry similar to 3R3P optimizations, it did not satisfy displacement criterion with the same input parameters. This suggests that the additional control of the 3R5P model that alters the transverse curvature contributed to the performance of the panel in the long-span application scenario.

Final selection of this geometry suggests that structural optimization alone may not be sufficient for identifying an appropriate configuration for curved mass timber shells. This study shows that many solutions achieved feasible structural performance and favorable material efficiency. However, wood-specific fabrication limitations through the curvature analysis and design considerations such as edge condition detail complexity, reveal meaningful differences in

real-world application practicality of a geometry and supports the addition of these tools in the digital workflow. Iteration 163 provided a balanced solution of feasible structural performance, efficient material use, and manufacturability through minimum curvature evaluation while also having a favorable panel-to-panel continuity. This suggests that the value of the optimization process lies not only in identifying a single high-performance configuration, but that it generates a population of high-performing alternatives for further fabrication, and architectural design criteria not explicitly included in the optimization objectives.

4.3 Prototyping and Fabrication

The first prototype fabricated at the 1:4 scale resulted in the identification of problems with the lamination process. Figure 45 in the appendix shows the digital to physical geometry analysis where it was identified that the panel was not meeting the bottom of the mold in the transverse direction. Inspection of the prototype and edge off-cuts found significant glue-line gaps suggesting inadequate pressure. However, the vacuum pressure gauge was noted to be within the appropriate pressure range of 21-25 inHg, prompting an adjustment to the fabrication process.

For the second 1:4 scale prototype, the x-configuration layup was tested using this adjusted fabrication process. By pre-bending the lamination layer and fastening them to the mold, it was ensured that the panel would reach the bottom of the mold. Figure 36 shows the results of this prototyping phase with the edge off-cut inspection finding no visible signs of glue line gaps. Although this finding suggests the refined fabrication process created a quality lamination, this visual inspection is highly limited and requires further study.



Figure 36. 1:4 scale prototype, X-configuration panel: physical panel (top) and edge off cut (bottom)

For the 1:1 scale prototype, the fabrication process began with the lamella bending feasibility check described in section 3.4. With height limits for the CNC machine used to fabricate the mold for the 1:1 panel the maximum displacement a lamella could be bent to was 5.75”. The maximum displacement of the lamella in the feasibility check was 21.5 cm or about 8.4”. This exceeded the maximum possible displacement needed to bend a lamella to the mold suggesting it was feasible to fabricate the panel. This was then confirmed with the successful fabrication of the 1:1 prototype (Figure 38). Pre-bending of the boards was done with relative ease and there was no need for additional equipment to achieve the lamination suggesting its potential manufacturability.

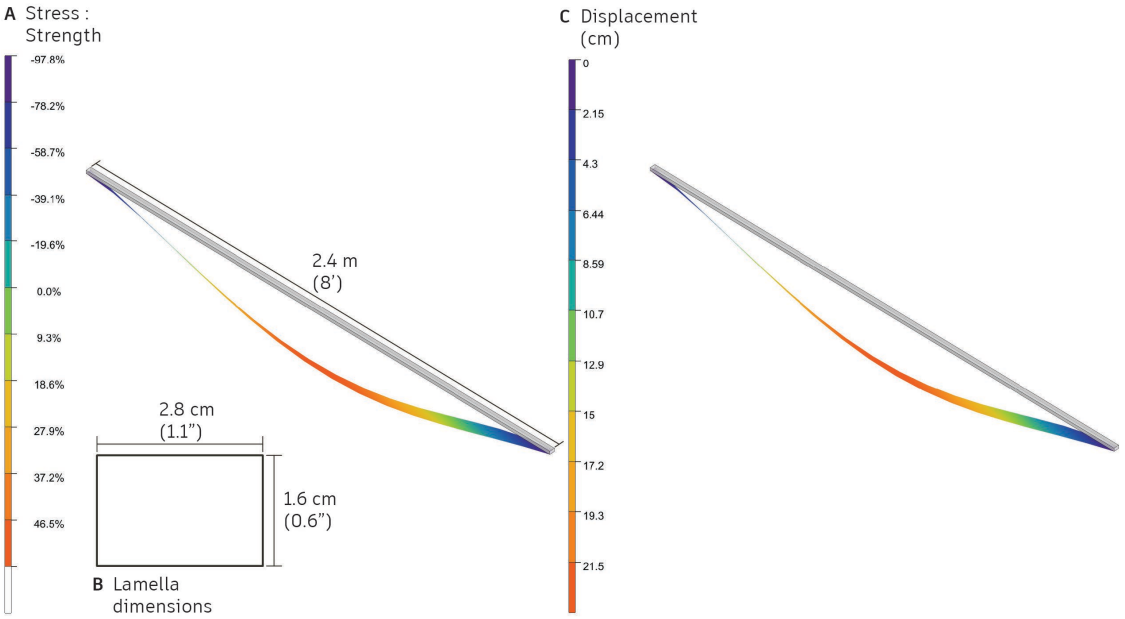


Figure 37. 1:1 lamella bending feasibility check: A.) stress: strength ratio approaching 100% B.) lamella dimensions C.) max displacement of 21 cm (8.4")

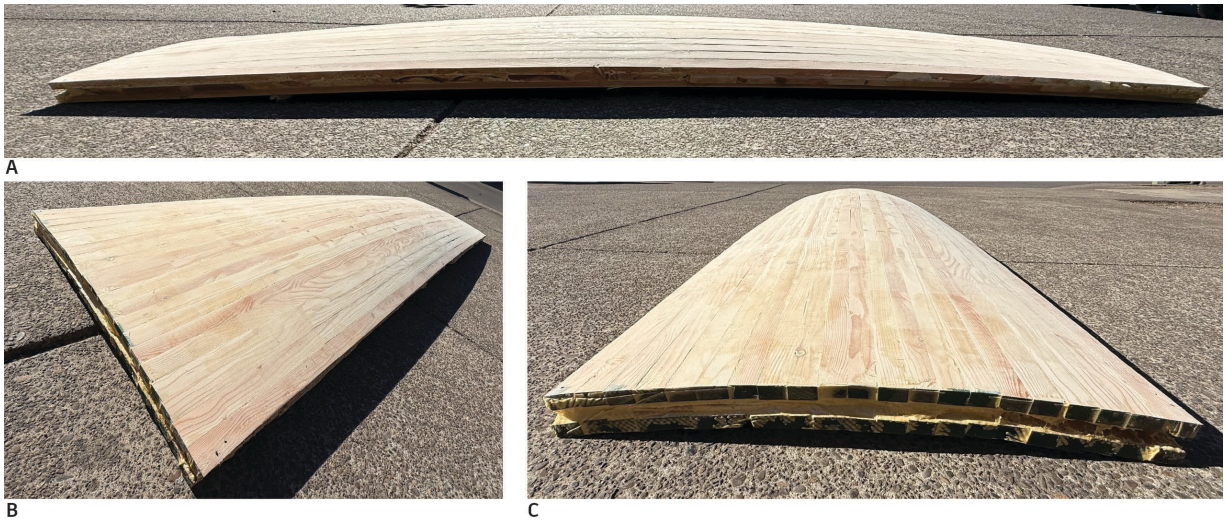


Figure 38. 1:1 physical prototype: A.) longitudinal view B.) perspective C.) transverse view

Visual comparison of the fabricated panel with the digital geometry showed a close correspondence between the intended and resulting curvature in both the longitudinal and transverse directions (Figure 50 in appendix). The physical panel maintained the overall doubly curved form of the digital model, with no visually apparent deviations that substantially altered the intended geometry. Importantly, the full-scale fabrication used lamella with dimensions classifying them as "thins" and "narrows", which were able to bend and twist into the required geometry while maintaining visually continuous contact between adjacent lamellae.

The fabrication process also employed commonly available tools and methods described in Section 3.4, and no observed stage of fabrication indicated an immediate limitation that would prevent the panel from being manufactured using this approach. These observations provide preliminary support for the manufacturability of the selected geometry and the use of thins and narrows within the curved CLT system; however, this assessment remains limited to visual inspection and the fabrication of a single panel. Additional dimensional analysis, evaluation of bond-line quality, structural testing, and repeated fabrication would be required before broader conclusions regarding geometric accuracy or manufacturing feasibility could be established.

4.4 Design and Material Implications

For the hypothetical design scenario, the final geometry was applied as a point supported system with three structural bays. Dividing the 110’ span into a central long span bay of 78.4’ (24 m) flanked by two 13.9’ (4.24 m) bays allows for variations in spatial scale to be created (Figure 39). For comparison with a typical rectilinear system, the volume of a 7-ply CLT (22.4 cm or 8.8”) panel was calculated for the same 24 m x 3 m area covered by the optimized panel (Figure 40). The volume comparison between the two is stark with flat panels having a total volume of 17.8 m^3 while the optimized thin shell panel has a volume of 10.3 m^3 or a 42% material reduction for the same area covered. This comparison shows the significant material savings by comparing the panels alone without considering the additional material needed to create the beams or additional columns needed in the post and beam system. The long-span application is particularly significant as increasing span magnifies material demands in rectilinear systems, providing a design condition which the structural advantages of shell geometry and material reduction can be more clearly evaluated.

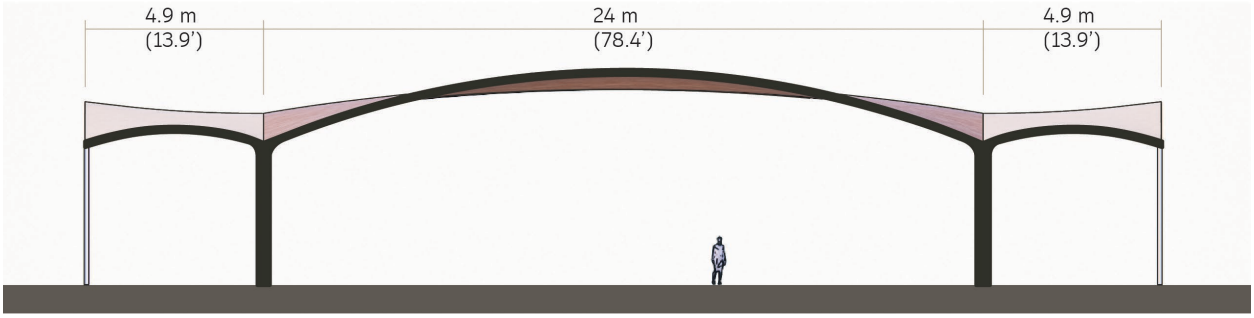


Figure 39. Airport section: shows 24 m optimized panel in the middle flanked by 4.24 m panels on each side

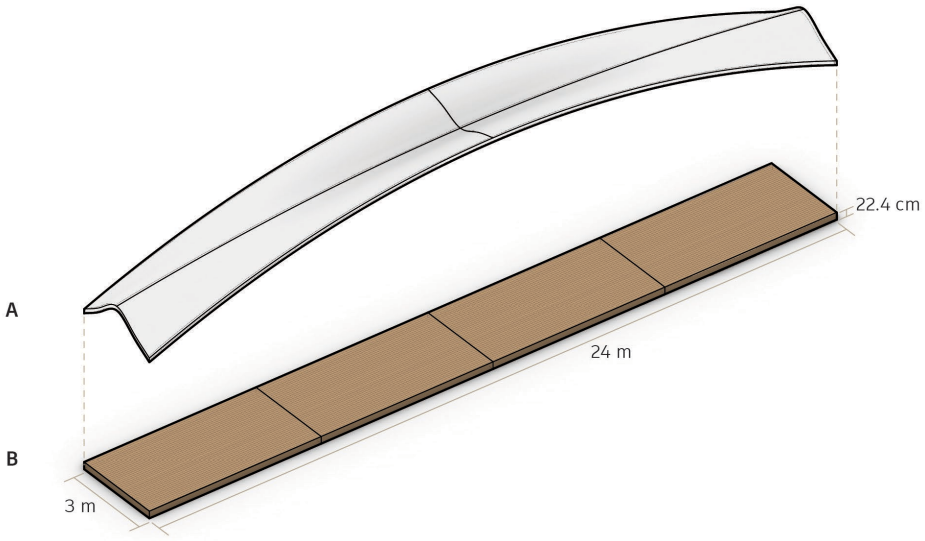


Figure 40. Volume comparison setup: A.) optimized airport panel with a volume of 10.3 m^3 B.) Flat 7-ply CLT panels with a volume of 17.8 m^3

When considered in relation to the material source investigated in this thesis, this comparison suggests a different approach to material efficiency than conventional mass timber construction. The CLT thin shell leverages geometry to achieve structural performance while reducing total wood volume, rather than relying on increasingly large structural members. By pairing the fiber source in the workflow, a designer can pair material and structural efficiency with underutilized fiber-sources. The resulting 42% reduction in wood volume represents more than reduced material, it demonstrates the potential for optimization of thin shell long-span CLT panels to increase the structural value obtained from "thins" and "narrows" produced from SDT. Additionally, this reduction highlights the competing objectives associated with the proposed fiber source from SDT, which is abundant, but a thin-shell system would use less of it. The results suggest the potential for an architectural and structural value-added application; however further study is needed to evaluate the economic value of this application.

CHAPTER V
CONCLUSION

5.1 Summary

This thesis presents a design and optimization workflow for CLT thin-shell panels using "thins" and "narrows" from SDT. Through a fiber-source-aware parametric geometry generation model, initial design structural analysis, multi-objective optimization, and integrated fabrication checks, this framework demonstrates the potential for a materially efficient, value-added application for an underutilized timber source. Throughout this study, 21,300 individual shells were analyzed through the lens of a hypothetical long-span design scenario intended to test the workflow as a design tool. Through a series of controlled filtration procedures, the workflow facilitated in analyzing large quantities of data to identify a single shell that met the established manufacturing feasibility metrics and material-efficiency objectives, addressing the research question posed in this thesis. When applied to the hypothetical long-span case study, the selected geometry used approximately 42% less wood compared to flat CLT panels covering the same area. Demonstrating, within the limits of design-phase analysis, that the dimensional properties of "thins" and "narrows" can be used in a materially efficient curved thin-shell CLT long-span system.

The results of this research demonstrate that a computational design and evaluation framework can be used to identify curved CLT shell geometries that balance structural performance, material efficiency, and fabrication constraints while considering the dimensional characteristics of thins and narrows derived from small-diameter timber. Through successive geometry generation, structural optimization, clustering, curvature evaluation, and physical fabrication, the framework reduced a broad design space to a selected shell geometry that satisfied the established structural and curvature criteria and was subsequently fabricated using the target material. The resulting prototype provides preliminary evidence that "thins" and "narrows" can accommodate the bending and twisting required by the selected geometry without visually apparent gaps between lamellae. While these findings do not establish broader manufacturing or structural feasibility for full-sized long-span curved CLT manufactured with "thins" and "narrows", they demonstrate the ability of the proposed framework to connect material constraints, computational design, structural evaluation, and fabrication in the development of curved mass timber systems.

5.2 Limitations and Future Work

With much of this study centered around the development of the multi-objective optimization that incorporated initial structural analysis, it's important to acknowledge the limits of these tools. Karamba gives a basis for initial design structural analysis but is currently no substitute for rigorous engineering analysis. Additionally, Karamba does not consider the complex internal structural relationship of cross laminated multi-ply material configurations or conduct plate theory analysis. These limits do not invalidate the results of the study, but as digital analysis tools continue to improve and become more accessible, future studies could explore incorporation of more robust analysis methods. Material properties used for the structural analysis were limited to Douglas fir; however, other species are harvested and produce small-diameter logs. With much variability in material properties between wood species, future studies could explore how different species in panels, or even between layers, impact the performance and geometry.

For analysis of the physical prototypes and models, evaluation was limited to visual inspection of the curved geometry and gluing conditions between layers. Future studies could do more precise measurement of glue lines or the gaps between lamellae. Additionally, incorporation of a digital-to-physical analysis into the digital workflow could provide a more robust quantitative comparison between the geometries. Assumptions made about balancing diagonal layup using the X-configuration could be explored further through destructive testing or through structural calculations.

This study evaluates material efficiency only at the scale of a specific structural system and does not evaluate economic value added to the SDT through use in these panels. Future work could explore manufacturing costs, product value, market demand, and production scale to determine if the use of less fiber has meaningful contributions towards broader SDT utilization.

5.3 Impact

This research establishes a framework for connecting the structural and fabrication potential of curved mass timber systems with the use of thins and narrows produced from small-diameter timber (SDT). Forest restoration and thinning practices generate material that can be difficult to incorporate into conventional high-value wood products, while mass timber provides an opportunity to retain wood within a long-lived building application and extend the environmental

benefits associated with timber construction. By incorporating the dimensional and fabrication characteristics of “thins” and “narrows” into a computational workflow that considers geometry, structural performance, material volume, curvature, and manufacturability, this thesis demonstrates a potential pathway for evaluating SDT material beyond conventional planar applications.

The fabrication study further provides preliminary evidence that actual “thins” and “narrows” can accommodate the bending and twisting required by the selected curved geometry. Additionally, being already milled into these thin and narrow dimensions reduces material waste from sawdust when compared to similar double-curved engineered wood products that cut standard dimensional lumber into sizes that are easier to bend and twist. Savings are also found by using thin lamella which achieves the curvature without needing to CNC boards into custom shaped slats. While additional research is necessary to establish structural performance, manufacturing scalability, and environmental benefits, the framework developed through this thesis provides a foundation for investigating how material generated through forest health initiatives could contribute to higher-value mass timber applications while expanding the design possibilities of curved timber construction.



Figure 41. Airport render exterior: showing how panels aggregate into the hypothetical airport layout



Figure 42. Airport render interior



Figure 43. Successful 1:1 panel fabrication: achieved double curvature with "thins" and "narrows" with no need of custom lamella shapes or specialty tools, displays minimal displacement when stood on and can be moved without the need of additional equipment

APPENDIX: PHYSICAL PROTOYPE FABRICATION PROCESS IMAGES



Figure 44. Diagonal layup layer for 1:4 scale prototype: masking tape keeps individual lamella in the correct order

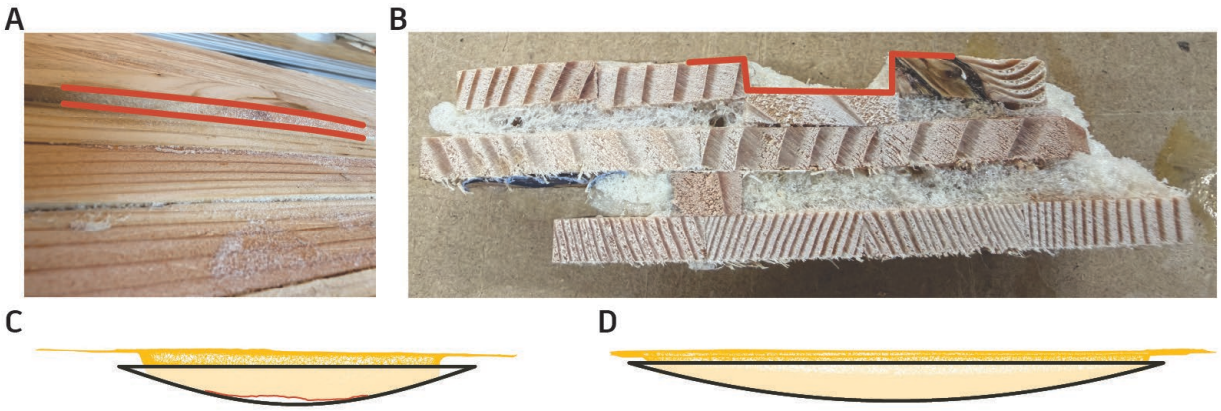


Figure 45. Identifying fabrication process problems: A.) top of panel at crown B.) edge off-cut corresponding with large glue-line gaps C.) transverse view of digital vs. physical (orange) geometry showing curvature deviations in the transverse crown area of the panel D.) longitudinal view of digital vs. physical (orange) geometry



Figure 46. Small fabrication process test: meant to test process of securing the panel to the mold prior to vacuum bag to improve lamination quality



Figure 47. X-configuration layer: used in the second 1:4 scale prototype, tape is added to hold the four quadrants of diagonal lamella together



Figure 48. Testing new fabrication process: securing the x-configuration panel to the mold prior to lamination



Figure 49. Process to secure 1:1 panel to the mold: using a wood mold negative, clamps are used to reduce the distance between lamella in the transverse direction while vertical clamps press the mold negative down



Figure 50.1:1 digital geometry vs. physical prototype comparison: finding no noticeable geometry difference upon visual inspection A.) transverse view B.) longitudinal view

REFERENCES CITED

[1] Edward Allen and Waclaw Zalewski. 2010. *Form and Forces: Designing Efficient, Expressive Structures*. John Wiley & Sons.

[2] Matthias Arnold, Philipp Dietsch, Roland Maderebner, and Stefan Winter. 2022. Diagonal Laminated Timber—Experimental, Analytical, and Numerical Studies on the Torsional Stiffness. *Constr. Build. Mater.* 322, (2022). https://doi.org/10.1016/j.conbuildmat.2022.126455

[3] Nadir Ayrilmis, Umit Buyuksari, and Nusret As. 2010. Bending strength and modulus of elasticity of wood-based panels at cold and moderate temperatures. *Cold Reg. Sci. Technol.* 63, 1–2 (2010), 40–43. https://doi.org/10.1016/j.coldregions.2010.05.004

[4] R. James Barbour. 1999. Relationship Between Diameter and Gross Product Value for Small Trees. 1999. .

[5] Simon Bechert, Lotte Aldinger, Dylan Wood, Jan Knippers, and Achim Menges. 2021. Urbach Tower: Integrative Structural Design of a Lightweight Structure Made of Self-Shaped Curved Cross-Laminated Timber. *Structures* 33, (2021), 3667–3681. https://doi.org/10.1016/j.istruc.2021.06.073

[6] Simon Bechert, Christoph Schlopschnat, Monika Göbel, Simon Aicher, Achim Menges, and Jan Knippers. 2025. livMatS Biomimetic Shell: Structural Advancements of Segmented Timber Shells Towards Permanent Building Constructions. *Structures* 79, (2025). https://doi.org/10.1016/j.istruc.2025.109524

[7] Sujit Bhandari, Erica C. Fischer, M.ASCE, Mariapaola Riggio, Lech Muszynski, and Sina Jahedi. 2024. Mechanical Characterization of Connections for Modular Cross-Laminated Timber Construction Using Underutilized Lumber. *J. Struct. Eng.* 150, 2 (2024).

[8] Sujit Bhandari, Mariapaola Riggio, Sina Jahedi, Erica C. Fischer, Lech Muszynski, and Zhixin Luo. 2023. A Review of Modular Cross Laminated Timber Construction: Implications for Temporary Housing in Seismic Areas. *J. Build. Eng.* 63, (2023). https://doi.org/https://doi.org/10.1016/j.jobe.2022.105485

[9] Zoltán Börcsök and Zoltán Pásztory. 2021. The Role of Lignin in Wood Working Processes Using Elevated Temperatures: An Abbreviated Literature Survey. *Eur. J. Wood Wood Prod.* 79, (2021), 511–526. https://doi.org/10.1007/s00107-020-01637-3

[10] Cajsa Carlson. 2022. Ascent Skyscraper in Milwaukee Becomes World's Tallest Timber Building. *Dezeen*. Retrieved August 8, 2026 from https://www.dezeen.com/2022/08/03/ascent-tower-milwaukee-worlds-tallest-timber-building/

[11] Galina Churkina, Alan Organschi, Christopher P. O. Reyer, Andrew Ruff, Kira Vinke, Zhu Liu, Barbra K. Reck, T.E. Graedel, and Joachim Schellnhuber. 2020. Buildings as a Global Carbon Sink. *Nat. Sustain.* 3, 4 (2020), 269–276.

[12] Pablo Crespell and Sylvain Gagnon. 2010. *Cross Laminated Timber: A Primer*. FPInnovations.

[13] Arnaud De Coster, Lars De Laet, and Tine Tysmans. 2024. Exploring the Three-Dimensional Space with Modular Concrete Shells: Form-Finding, Design and Structural Analysis. *Thin-Walled Struct.* 195, (2024), 111336. https://doi.org/10.1016/j.tws.2023.111336

[14] Tomás Mendez Echenagucia, N B Roozen, and Philippe Block. 2016. Minimization of Sound Radiation in Doubly Curved Shallow Shells by Means of Structural Stiffness. In *Spatial Structures in the 21st Century*, 2016. IASS.

[15] W H Emmingham and D Green. 1984. *Thinning Systems for Western Oregon Douglas-fir Stands*. Oregon State University Extension Services.
[16] Thomas Fahey. 1983. Product Recovery from Hemlock “Pulpwood” from Alaska. *PNW-RP-303* (1983).
[17] FAO. 2025. *Global Forest Products Facts and Figures 2024*. Food and Agriculture Organization of the United Nations.
[18] Fangwei Fu, Haiqing Ren, Fengwu Liu, Chao Liu, Lijun Wang, and Yong Zhong. 2024. A High-Strength Laminate Made of Small-Diameter Plantation Wood: Flatwise Bending Mechanical Properties. *Ind. Crops Prod.* 219, (2024). https://doi.org/10.1016/j.indcrop.2024.119108
[19] Milan Gaff, Vojtěch Vokatý, Marian Babiak, and Bekir Cihad Bal. 2016. Coefficient of Wood Bendability as a Function of Selected Factors. *Constr. Build. Mater.* 126, (2016), 632–640. https://doi.org/10.1016/j.conbuildmat.2016.09.085
[20] Julia Gómez Goenaga, Aurora Monge-Barrio, Karla Saldaña Ochoa, and Antonio Villanueva Peñalver. 2026. Digital Workflows for Informed Decision Making in Building Envelope Design: A Systematic Literature Review. *Appl. Soft Comput.* 187, (2026). https://doi.org/10.1016/j.asoc.2025.114377
[21] David W. Green, Eini C. Lowell, and Roland Hernandez. 2005. Structural Lumber from Dense Stands of Small-Diameter Douglas-Fir Trees. *For. Prod. J.* 55, 7/8 (2005).
[22] Ryan Haugo, Chris Zanger, Tom DeMeo, Chris Ringo, Ayn Shlisky, Kori Blankenship, Mike Simpson, Kim Mellen-McLean, Jane Kertis, and Mark Stern. 2015. A New Approach to Evaluate Forest Structure Restoration Needs Across Oregon and Washington, USA. *For. Ecol. Manag.* 335, (2015), 37–50. https://doi.org/10.1016/j.foreco.2014.09.014
[23] Shane Hossell, Will Hawkins, Antony Darby, and Tim Ibell. 2024. Timber Groin Vault Floor System for Low Embodied Carbon Buildings. In *Redefining the Art of Structural Design*, 2024. IASS.
[24] Shane Hossell, Will Hawkins, Antony Darby, Tim Ibell, and Nicola Lines. 2023. Timber Vaults for Ultra-Low-Carbon Building Structures. In *World Conference on Timber Engineering (WCTE 2023)*, 2023. WCTE, Oslo, Norway, 3475–3484. https://doi.org/10.52202/069179-0452
[25] Rebecca E Ibach. 2021. *Wood Handbook: Wood as an Engineering Material. Chapter 19: Specialty Treatments*. Forest Product Labratory.
[26] Sina Jahedi, Lech Muszynski, Mariapaola Riggio, Benjamin Belengino, and Sujit Bhandari. 2022. MOE Distribution in Visually Graded Ponderosa Pine Lumber Harvested from Restoration Programs in Southern Oregon and Northern California. *Wood Fiber Sci.* 54, 2 (2022), 90–98. https://doi.org/https://doi.org/10.22382/wfs-2022-10
[27] Sina Jahedi, Lech Muszynski, Mariapaola Riggio, and Sujit Bhandari. 2023. Bending Characteristics of Custom CLT Layups Laminated with Ponderosa Pine Harvested from Restoration Programs. *Wood Fiber Sci.* 55, 3 (2023), 282–294. https://doi.org/https://doi.org/10.22382/wfs-2023-23
[28] Günther Jauk. 2021. Cross-Laminated Timber Reinvented: Holzbau Unterrainer is a Specialist in Curved CLT. *Timber Online*. Retrieved November 17, 2025 from https://www.timber-online.net/content/holz/holzkurier/en/wood_products/2021/07/cross-laminated-timber-reinvented.html
[29] Mohammad Kader, Mohammad Alzuhaili, Ivan Markov, D Markov, and Mohammad Al Zuhaili. 2018. Structural Optimization for Axisymmetric Shells of Revolution Structures by

Finite Element Method. Thesis for PhD. University of Architecture Civil Engineering and Geodessy. https://doi.org/10.13140/RG.2.2.19159.65442
[30] Erol Karacabeyli (Ed.). 2013. *CLT handbook: Cross-Laminated Timber* (U.S. edition ed.). FPInnovations, Pointe-Claire, QC.
[31] Naresh Khanal, Woodam Chung, John Hogland, Yong Chen, and Andres Susaeta. 2026. Economic Impacts of Mass Timber Production Using Small-Diameter Wood from Fuel Reduction and Restoration Treatments in Eastern Oregon. *Trees For. People* 26, (2026). https://doi.org/10.1016/j.tfp.2026.101417
[32] Anja Kunic, Davide Angeletti, Giuseppe Marrone, and Roberto Naboni. 2024. Design and Construction Automation of Reconfigurable Timber Slabs. *Autom. Constr.* 168, (2024). https://doi.org/https://doi.org/10.1016/j.autcon.2024.105872
[33] Shaghayegh Kurzinski and Paul L. Crovella. 2024. Investigating the Out-of-Plane Bending Stiffness Properties in Hybrid Species Diagonal-Cross-Laminated Timber Panels. *Appl. Sci.* 14, 7 (2024), NA-NA. https://doi.org/10.3390/app14072718
[34] Braden Lawrie. 2025. Mass VeneerX: Multi-Performance Optimization of Veneer-Based Mass Timber Panels. Thesis for Masters. University of Oregon.
[35] Livingston LeVan. 2001. Exploring the Uses for Small-Diameter Trees. *For. Prod. J.* 51, 9 (2001).
[36] LOCTITE. 2023. Loctite HB X302 Purbond NA. Retrieved from https://gated.datasheets.tdx.henkel.com/gated/LOCTITE-HB-X302-PURBOND-NA-en_US.pdf
[37] Simon Lux, Johannes Konnerth, and Andreas Neumüller. 2025. Mechanical Properties of Strip-Like Laminations Made from Hardwood. *Eur. J. Wood Wood Prod.* 83, (2025), 90. https://doi.org/10.1007/s00107-025-02246-8
[38] Musaab Mahjoub. Awatif CLT Analysis. Retrieved August 9, 2026 from https://awatif.co/clt/
[39] Paul Mayencourt. 2022. Mass Reduction: Opportunities and Structural Optimization Methods to Reduce Material Use in Mass Timber Buildings. Thesis for PhD. Massachusetts Institute of Technology.
[40] Abhijeet Mishra, Florian Humpenöder, Galina Churkina, Christopher P. O. Reyer, Felicitas Beier, Benjamin Leon Bodirsky, Hans Joachim Schellnhuber, Hermann Lotze-Campen, and Alexander Popp. 2022. Land use Change and Carbon Emissions of a Transformation to Timber Cities. *Nat. Commun.* 13, 1 (2022). https://doi.org/10.1038/s41467-022-32244-w
[41] Mostafa Mohammadabadi, Jordan Miller, Jason Street, Yunsang Kim, and Kevin Ragon. 2023. Wood-Based Corrugated Core Sandwich Panels Manufactured Using a Wooden Mold. *BioResources* 18, 2 (2023), 3033–3043. https://doi.org/10.15376/biores.18.2.3033-3043
[42] Lech Muszynski. 2023. ‘Eat the Problem’ or a Case for Use of Small-Diameter Logs in Specialty Mass-Timber Panels. *International Mass Timber Conference*. Retrieved November 4, 2025 from https://masstimberconference.com/report/content/eat-the-problem-or-a-case-for-use-of-small-diameter-logs-inspecialty-mass-timber-panels/
[43] Dung Ngo and Eric Pfeiffer. 2003. *Bent Ply the Art of Plywood Furniture* (1st ed.). Princeton Architectural Press, New York.
[44] David. Nicholls. 2010. *Alaska Birch for Edge-Glued Panel Production—Considerations for Wood Products Manufacturers*. U.S. Department of Agriculture, Forest Service, Pacific Northwest Research Station, Portland, OR. https://doi.org/10.2737/PNW-GTR-820

[45] Malcolm P. North, Ryan E. Tompkins, Alexis A. Bernal, Brandon M. Collins, Scott L. Stephens, and Robert A. York. 2022. Operational Resilience in Western US Frequent-Fire Forests. *For. Ecol. Manag.* 507, (2022). https://doi.org/10.1016/j.foreco.2021.120004
[46] Edward C. Peck. 1956. *Bending Solid Wood to Form*. U.S. Department of Agriculture, Forest Service, Forest Products Laboratory, Madison, WI.
[47] Maximilian Pramreiter, Tobias Nenning, Christian Huber, Ulrich Müller, Benjamin Kromoser, Paul Mayencourt, and Johannes Konnerth. 2023. A Review of the Resource Efficiency and Mechanical Performance of Commercial Wood-Based Building Materials. *Sustain. Mater. Technol.* 38, (2023). https://doi.org/10.1016/j.susmat.2023.e00728
[48] Michael H. Ramage, Henry Burridge, Marta Busse-Wicher, George Fereday, Thomas Reynolds, Darshil U. Shah, Guanglu Wu, Li Yu, Patrick Fleming, Danielle Densley-Tingley, Julian Allwood, Paul Dupree, P. F. Linden, and Oren Scherman. 2017. The Wood from the Trees: The Use of Timber in Construction. *Renew. Sustain. Energy Rev.* 68, 1 (2017), 333–359. https://doi.org/10.1016/j.rser.2016.09.107
[49] Ekkehard Ramm, Kai-Uwe Bletzinger, and Reiner Reitinger. 1993. Shape Optimization of Shell Structures. *Int. Assoc. Shell Spat. Struct.* 2, 3 (1993), 377–398.
[50] Mario Ramos-Maldonado, Cristhian Aguilera-Carrasco, Mario Ramos-Maldonado, and Cristhian Aguilera-Carrasco. 2021. Trends and Opportunities of Industry 4.0 in Wood Manufacturing Processes. In *Engineered Wood Products for Construction*. IntechOpen. https://doi.org/10.5772/intechopen.99581
[51] Christopher Robeller, Seyed Sina Nabaei, and Yves Weinand. 2014. Design and Fabrication of Robot-Manufactured Joints for a Curved-Folded Thin-Shell Structure Made from CLT. In *Robotic Fabrication in Architecture, Art and Design*. Springer International Publishing, Cham, 67–81. https://doi.org/10.1007/978-3-319-04663-1_5
[52] Daniel Jonas Roche. 2023. Cross-laminated timber (CLT) turns 100. *The Architect's Newspaper*. Retrieved October 19, 2025 from https://www.archpaper.com/2023/08/cross-laminated-timber-clt-turns-100/
[53] Robert Ross. 2021. *Wood Handbook: Wood as an Engineering Material*. USDA and USFS.
[54] RS&H. *EUG Advanced Terminal Planning Executive Summary*.
[55] Moritz Sanne, Gudrun Ahn-Ercan, and Alexander Pfriem. 2020. A Mathematical Solution for Calculating the Springback of Laminated Beech Stacks Molded within the Elastic Range. *Forests* 11, 7 (July 2020). https://doi.org/10.3390/f11070725
[56] Gerhard Schickhofer and Werner Guggenberger. 1994. Strarrer und Nachgiebiger Verbund Bei Geschichteten Flachenhaften Holzstrukturen. Thesis for PhD. Graz University.
[57] Thomas Sensenig, John D. Bailey, and John C. Tappeiner. 2013. Stand Development, Fire and Growth of Old-Growth and Young Forests in Southwestern Oregon, USA. *For. Ecol. Manag.* 291, (2013), 96–109. https://doi.org/10.1016/j.foreco.2012.11.006
[58] Georg Stecher, Roland Maderebner, Philipp Zingerle, and Michael Flach. 2016. Curved Cross-Laminated Timber Elements. In *World Conference on Timber Engineering*, 2016. WCTE, Viena, Austria.
[59] William Cornwall Stevens and N Turner. 1970. *Wood Bending Handbook*. Woodcraft Suply Co, Woburn Massachuusettes.
[60] Tom Svilans. 2021. GluLamb: A Toolkit for Early-Stage Modelling of Free-Form Glue-Laminated Timber Structures. 2021. Ixia, Rhodes, Greece, 373–380. https://doi.org/10.35490/EC3.2021.194

[61] Thomas Tannert, AnnaLisa Meyboom, Oliver Neumann, and Iain Macdonald. 2015. *Shell Structures in Wood*. University of British Colombia. Retrieved from https://www.bcfii.ca/wp-content/uploads/2021/02/fii418-2014-15-ubc-cawp-shell-structures-in-wood-1.pdf
[62] Artur de Vito, William Vicente, and Yi Min Xie. 2023. Topology Optimization Applied to the Core of Structural Engineered Wood Product. *Structures* 48, (2023). https://doi.org/https://doi.org/10.1016/j.istruc.2023.01.036
[63] Xinyu Wang, Changdong Zhang, Tingting Liu, Wenhe Liao, and Cong Wang. 2022. Variable-Thickness Optimization Method for Shell Structures Based on a Regional Evolutionary Control Strategy. *Thin-Walled Struct.* 172, (2022), 108848. https://doi.org/10.1016/j.tws.2021.108848
[64] Christopher Wilk. 2017. *Plywood a Material Story*. V & A Publishing.
[65] Thomas Wortmann. 2017. Opossum. In *Opossum: Introducting and Evaluating a Model-Based Tool for Grasshopper*, 2017. CADDRIA, Hong Kong.
[66] Juan S Zambrano-Jaramillo, Erica C Fischer, and Dylan Wood. 2024. Geometry, Material, and Structural Exploration for Curved Cross- Laminated Timber Structures. In *International Association for Shell and Spatial Structures*, 2024. IASS, Zurich, Switzerland.
[67] 1858. Wood Bending. *Scientific American*. Retrieved October 19, 2025 from https://www.scientificamerican.com/article/wood-bending-1858-05-01/
[68] 2000. *Forest Products Laboratory Research Program on Small-Diameter Material.* U.S. Department of Agriculture, Forest Service, Forest Products Laboratory, Madison, WI. https://doi.org/10.2737/FPL-GTR-110
[69] 2017. Toranoko Nursery / Takashige Yamashita Office. *ArchDaily*. Retrieved November 17, 2025 from https://www.archdaily.com/805198/toranoko-nursery-takashige-yamashita-office
[70] 2020. ANSI+117-2020-Standard Specifications for Structural Glued Laminated Timber of Softwood Species.
[71] 2021. Elephant House Zoo Zürich / Markus Schietsch Architekten. *ArchDaily*. Retrieved November 17, 2025 from https://www.archdaily.com/770772/elephant-house-zoo-zurich-markus-schietsch-architekten
[72] 2023. Wood Innovations Success Story: Small-Diameter CLT. FS-1161(x), (2023).
[73] 2024. *The Glulam Handbook: Facts About Glulam* (1:2024 ed.). Swedish Wood, Stockholm, Sweden.
[74] 2025. ANSI/APA PRG 320-2025 Standard for Performance-Rated Cross-Laminated Timber.
[75] TripleWood. Retrieved November 19, 2025 from https://www.triplewood.eu/en/projects/elephant-house-zoo-zurich
[76] EN 1995-1-1: Eurocode 5: Design of timber structures - Part 1-1: General - Common rules and rules for buildings. Retrieved February 25, 2026 from https://www.phd.eng.br/wp-content/uploads/2015/12/en.1995.1.1.2004.pdf